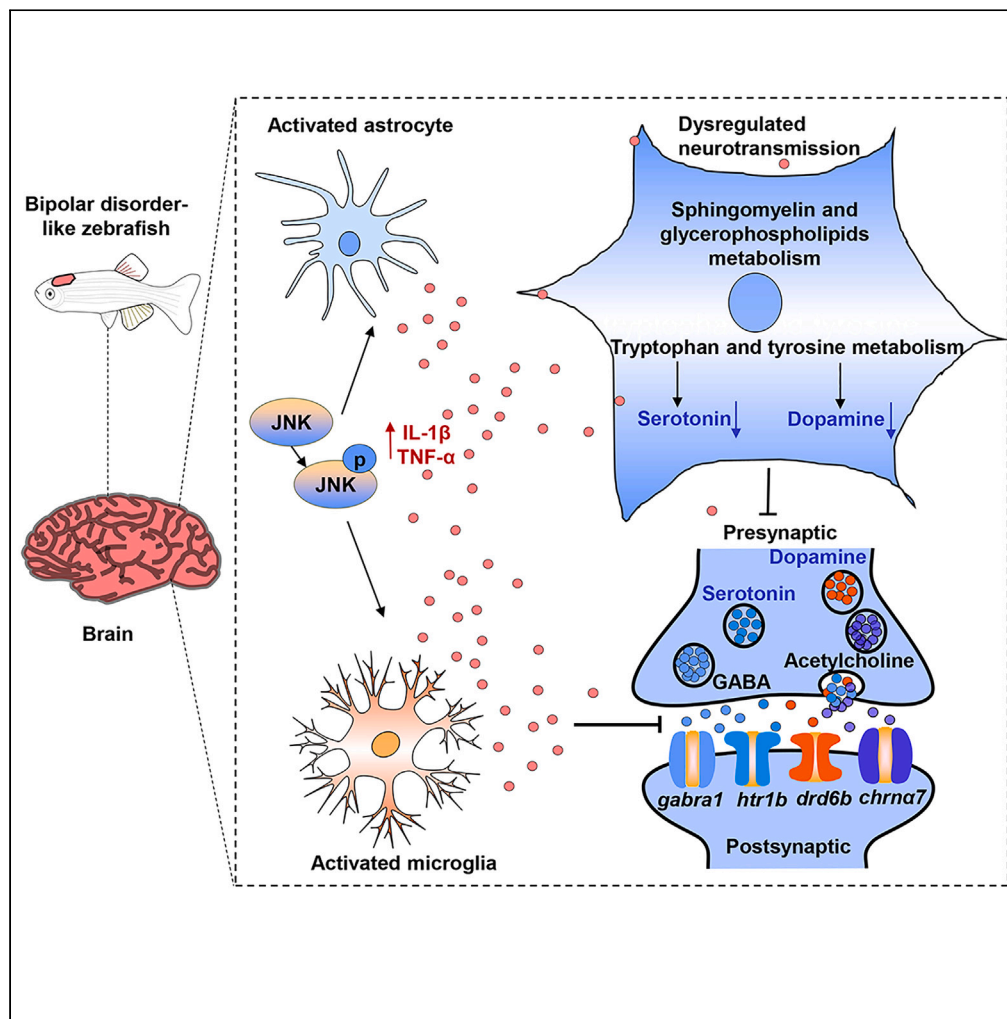


Article

Multi-omics analysis of a drug-induced model of bipolar disorder in zebrafish



Yameng Li, Lin Zhang, Mingcai Mao, ..., Xiyan Mu, Yongzhong Qian, Jing Qiu

qianyongzhong@caas.cn (Y.Q.)
qiuqing@caas.cn (J.Q.)

Highlights

A comprehensive disturbance of neurotransmission in bipolar disorder zebrafish

Alterations in synaptic transmission supported the observed behavioral phenotypes

These deficits were explained by a remodeling of amino acid and lipid metabolism

These alterations were associated with JNK-mediated neuroinflammation

Li et al., iScience 26, 106744
May 19, 2023 © 2023 The Author(s).
<https://doi.org/10.1016/j.isci.2023.106744>

Article

Multi-omics analysis of a drug-induced model of bipolar disorder in zebrafish

Yameng Li,¹ Lin Zhang,¹ Mingcai Mao,¹ Linjuan He,¹ Tiancai Wang,¹ Yecan Pan,¹ Xiaoyu Zhao,¹ Zishu Li,¹ Xiyan Mu,¹ Yongzhong Qian,^{1,*} and Jing Qiu^{1,2,*}

SUMMARY

Emerging studies demonstrate that inflammation plays a crucial role in the pathogenesis of bipolar disorder (BD), but the underlying mechanism remains largely unclear. Given the complexity of BD pathogenesis, we performed high-throughput multi-omic profiling (metabolomics, lipidomics, and transcriptomics) of the BD zebrafish brain to comprehensively unravel the molecular mechanism. Our research proved that in BD zebrafish, JNK-mediated neuroinflammation altered metabolic pathways involved in neurotransmission. On one hand, disturbed metabolism of tryptophan and tyrosine limited the participation of the monoamine neurotransmitters serotonin and dopamine in synaptic vesicle recycling. On the other hand, dysregulated metabolism of the membrane lipids sphingomyelin and glycerophospholipids altered the synaptic membrane structure and neurotransmitter receptors (*chrn α 7*, *htr1b*, *drd5b*, and *gabra1*) activity. Our findings revealed that disturbance of serotonergic and dopaminergic synaptic transmission mediated by the JNK inflammatory cascade was the key pathogenic mechanism in a zebrafish model of BD, provides critical biological insights into the pathogenesis of BD.

INTRODUCTION

Nearly 1%–3% of the population worldwide is affected by bipolar disorder (BD),¹ a serious mood disorder characterized by periodic episodes of depression and either mania (bipolar I disorder) or hypomania (bipolar II disorder and cyclothymic disorder).^{2,3} A systematic review and meta-analysis has shown that BD usually occurs in late adolescence or early adulthood,⁴ with the incidence of bipolar I disorder being similar in males and females, whereas bipolar II disorder occurring more frequently in females.^{5,6} Reports published to date indicate that the proportion of adults exhibited symptoms of anxiety or depression increased (from 36.4% to 41.5%) during the COVID-19 pandemic.⁷ In addition, BD patients had significantly higher levels of pandemic-related subjective cognitive dysfunction, which was particularly associated with symptoms, such as depression and anxiety.⁸ The World Mental Health Survey Initiative reported that the lifetime and 12-month prevalence of BD are approximately 2.4% and 1.5%, respectively,⁹ making it a chronic mental illness that often requires continuous monitoring and lifelong treatment and imposes a substantial economic burden on health care systems and society.¹⁰ However, the majority of the psychotropic medication (e.g., quetiapine) currently used for people with BD are developed for the treatment of other brain disorders such as schizophrenia,¹¹ and the preferred drug lithium has a relatively slow onset of action and a high number of adverse effects.¹²

At present, the importance of changes in brain structure¹³ and glial cell function,¹⁴ alterations in synaptic transmission,¹⁵ mitochondrial dysfunction¹⁶ and inflammation¹⁷ in BD has been emphasized in several studies on the pathogenesis of BD. In particular, BD can be divided into the following four pathways: dendritic spine aberrations and brain demyelination–altered neuronal synaptic plasticity,¹⁸ imbalance of excitatory/inhibitory transmission caused by the dysfunction of monoaminergic and glutamatergic,¹⁹ inadequate mitochondrial energy supply affected synaptic transmission²⁰ and inflammation activated by NF- κ B, mitogen-activated protein kinase (MAPK), and other inflammatory factors.^{21,22} Despite the known contribution of these pathways in BD, studies of BD pathogenesis have been mostly limited to one single type of molecular signature, and the relationship among these molecular pathways has not been elucidated. Thus, the molecular mechanisms involved in the initiation and progression of BD and the role of alterations in synaptic transmission and inflammation responses remain largely unknown.

¹Key Laboratory of Agri-food Quality and Safety of Ministry of Agriculture and Rural Affairs, Institute of Quality Standard and Testing Technology for Agro-Products, Chinese Academy of Agricultural Sciences, Beijing 100081, China

²Lead contact

*Correspondence: qianyongzhong@caas.cn (Y.Q.), qiuqing@caas.cn (J.Q.)
<https://doi.org/10.1016/j.isci.2023.106744>



Zebrafish (*Danio rerio*) is an important model system for studying BD because it is highly sensitive to acute or chronic stressful situations, and it exhibits powerful affective phenotypes similar to that of humans, including depression, anxiety, cognitive impairment, and manic-like behavior.^{23,24} A systematic review and meta-analysis have shown that existing well-established behavioral analysis methods for zebrafish support easy measurement of BD-related characteristic phenotypes (e.g., hyperactivity, depression, impaired memory, and social competence) on this model organism.²⁵ In addition, the structure and function of the central nervous system (CNS) in zebrafish are similar to that of mammals, and zebrafish has a high degree of physiological and genetic homology with humans.²⁶ However, there are also some limitations to the BD zebrafish model, such as the relatively small head sample size and the presence of duplicate genes.²⁷ Previous reports have confirmed that zebrafish can be used to model brain disorders such as depression²⁸ and schizophrenia,²⁹ and it can provide a more in-depth perspective on corresponding human disorders and their molecular pathogenesis.²³ Thus, characterizing molecular studies using BD zebrafish models could contribute to the elucidation of the evolutionarily conserved pathogenesis of BD and exploration of potentially effective therapeutic targets.

Therefore, comprehensive analysis focusing on the brain in healthy and diseased states is necessary to obtain comprehensive understanding of the molecular mechanism of BD. We performed high-throughput multi-omic profiling of female zebrafish brain tissue, including metabolomics, lipidomics, and transcriptomics; ultrastructural analysis using transmission electron microscopy (TEM) and synaptic functional studies. Additionally, we discovered that BD zebrafish had a unique metabolic profile, accompanied by marked abnormalities in synaptic structure, synaptic transmission dysfunction, and the development of neuroinflammation. These integrated biological pathways and other multi-level information on the molecular mechanism of BD could be used to identify potential treatments to rescue progressive metabolic dysfunction and synaptic damage in the early stages of BD.

RESULTS

Characteristics of the zebrafish model of BD

For our research, we opted to utilize a zebrafish model of BD induced by ciprofloxacin. This choice was motivated, in large part, by previous reports suggesting a link between gut microbiome alterations and BD.^{30,31} Furthermore, ciprofloxacin, a fluoroquinolone antibiotic, hinders DNA synthesis and replication, resulting in bacterial death. Improper use of this antibiotic during treatment may lead to gut dysbiosis and microbial imbalance.³² Clinical data have indicated that ciprofloxacin induces antibiotic mania,^{33,34} although the underlying mechanism remains unclear. Based on this research background, we hypothesized that ciprofloxacin-induced BD-like behavior in zebrafish could be attributed to disturbances in the microbiome-gut-brain axis. To verify this hypothesis, we utilized ciprofloxacin and generated a drug-induced BD-like zebrafish model and elucidated its molecular characteristics. The results of the locomotor trajectory plots and heat maps showed that zebrafish in the treatment groups exhibited more wall-hugging behavior in the horizontal position preference test (Figure 1A) and less exploratory behavior in the vertical position preference test (Figure 1B) compared with the control group. The behavioral phenotype of zebrafish in the high-concentration group was characterized by a significant addition in the distance traveled and manic-like behavior (Figures 1C, 1D, and S4), as well as a significant reduction in the total duration and frequency of movement to the central (Figure 1E) and top zones (Figure 1F). However, it is evident in the low-concentration group, except for a significant decrease in the frequency of movement to the central zones (Figure 1E). These findings indicated that zebrafish in the high-concentration treatment group showed BD-like behavior (hyperactivity, manic, depression, and anxiety), consistent with the behavior of previous mammalian BD models,^{35,36} indicating the effectiveness of this strategy in inducing BD in zebrafish. Furthermore, we found no significant differences in locomotor distance and frequency of occurrence of manic-like behavior in the treated zebrafish after a two-week treatment with lithium carbonate compared to the controls (Figures S5A–S5C). These results further validated that CIP-induced BD-like zebrafish can be used as a biological model for this disease.

In determining whether there were significant phenotypic differences between the BD zebrafish induced by the high-concentration treatment group and the control zebrafish, we performed a histopathological evaluation of zebrafish brains to investigate the pathological mechanism of BD. hematoxylin-eosin (HE)staining analysis showed a lack of structural integrity in the midbrain of BD zebrafish compared with that in the controls (Figure 2A). Additionally, Nissl staining revealed reduction in the number of neuronal cell bodies, while the neurons became round and larger than normal, indicating cell swelling (Figures 2B and 2C).

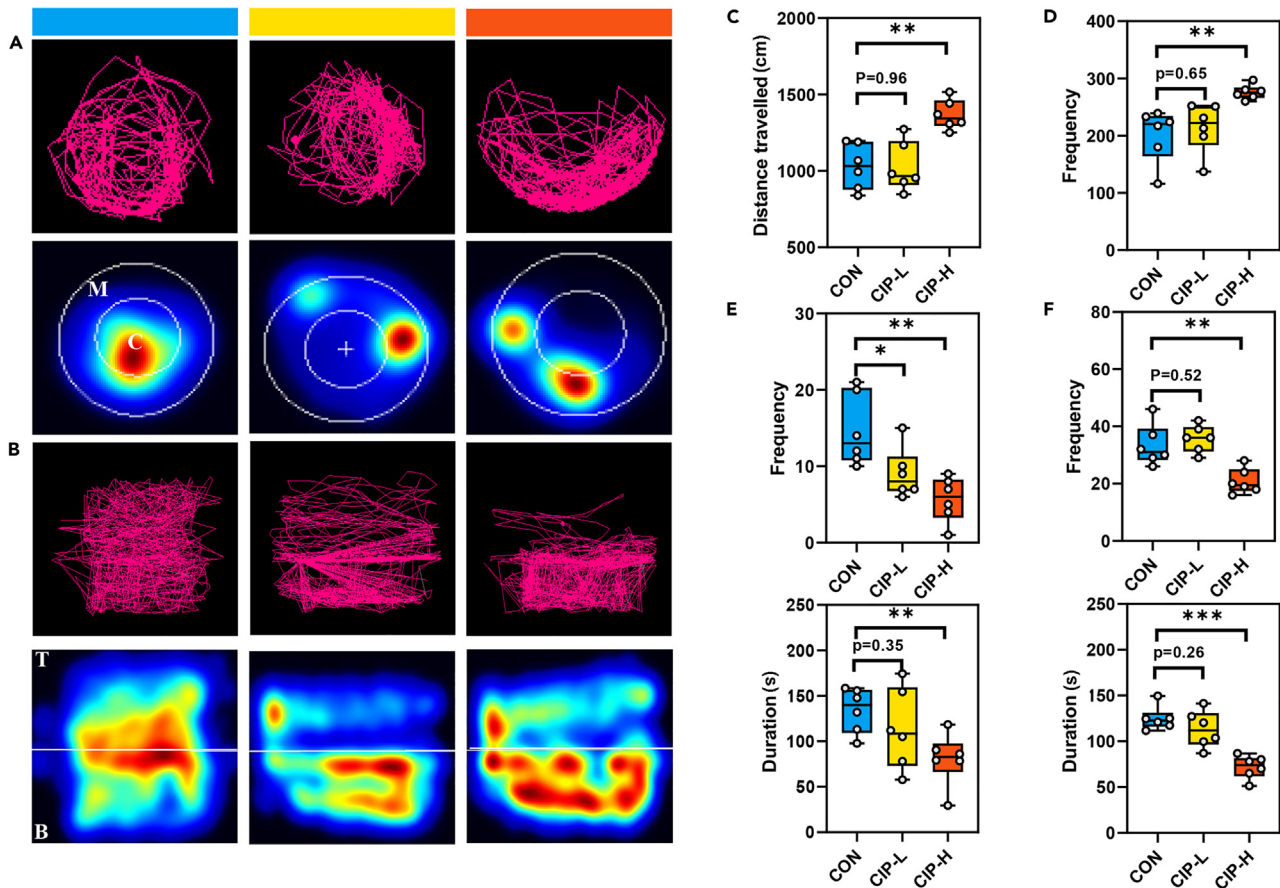


Figure 1. Behavioral phenotypes of control (CON) versus zebrafish model of BD

We tracked the swimming behavior of zebrafish within 5 min, covering the swimming trajectory, frequency of occurrence of manic-like behavior, total duration and frequency of movement to the top and central zones (CON, Zebrafish were reared in clear water for 4 weeks, $n = 6$; CIP-L, zebrafish were exposed to 100 µg/L concentration levels of ciprofloxacin for 4 weeks, $n = 6$; CIP-H, zebrafish were exposed to 1000 µg/L concentration levels of ciprofloxacin for 4 weeks, $n = 6$).

(A and B) Representative locomotor trajectory plots and heat maps of zebrafish in the horizontal (A) and vertical (B) position preference test (C, central zone; M, marginal zone; T, top zone; B, bottom zone).

(C–E) Box and Whisker plots of distance travelled (C), frequency of manic-like behavior (D) and total duration and frequency of movement to the central zones (E) in zebrafish in the horizontal position preference test.

(F) Box and Whisker plots of total duration and frequency of movement to the top zones in zebrafish in the vertical position preference test. Data are shown as mean \pm SEM, * $p < 0.05$, ** $p < 0.01$, *** $p < 0.001$, unpaired two-tailed Student's *t* test.

Consistent with the reduction in Nissl bodies, we found reduced expression of the neuron-specific antibody NeuN (Figures 2D, 2E, and 2F). Collectively, these results indicated pathological changes in the brain of BD zebrafish, with neuronal loss, cytosolic swelling, and morphological alterations as the main pathological features.

Multi-omic molecular profiles discriminate BD from controls

Metabolite and lipid profiling were performed using mass spectrometry and transcript analysis by RNA-sequencing. The clustering heatmap showed that a high percentage of metabolites were downregulated with the upregulation of lipids and genes in BD (Figure 3A). In addition, we observed that 35% (234) of the 661 metabolites identified were obviously altered, of which 62 were significantly upregulated and 172 were significantly downregulated (Figure 3B, Table S3). Moreover, 39% (253) of the 643 lipids showed differential variation in BD, of which 154 lipids were significantly upregulated and 99 lipids were significantly downregulated (Figure 3B, Table S4). Furthermore, 33% (10506) of the 32057 transcripts were differentially expressed in BD, of which 7890 transcripts were significantly upregulated and 2616 transcripts were

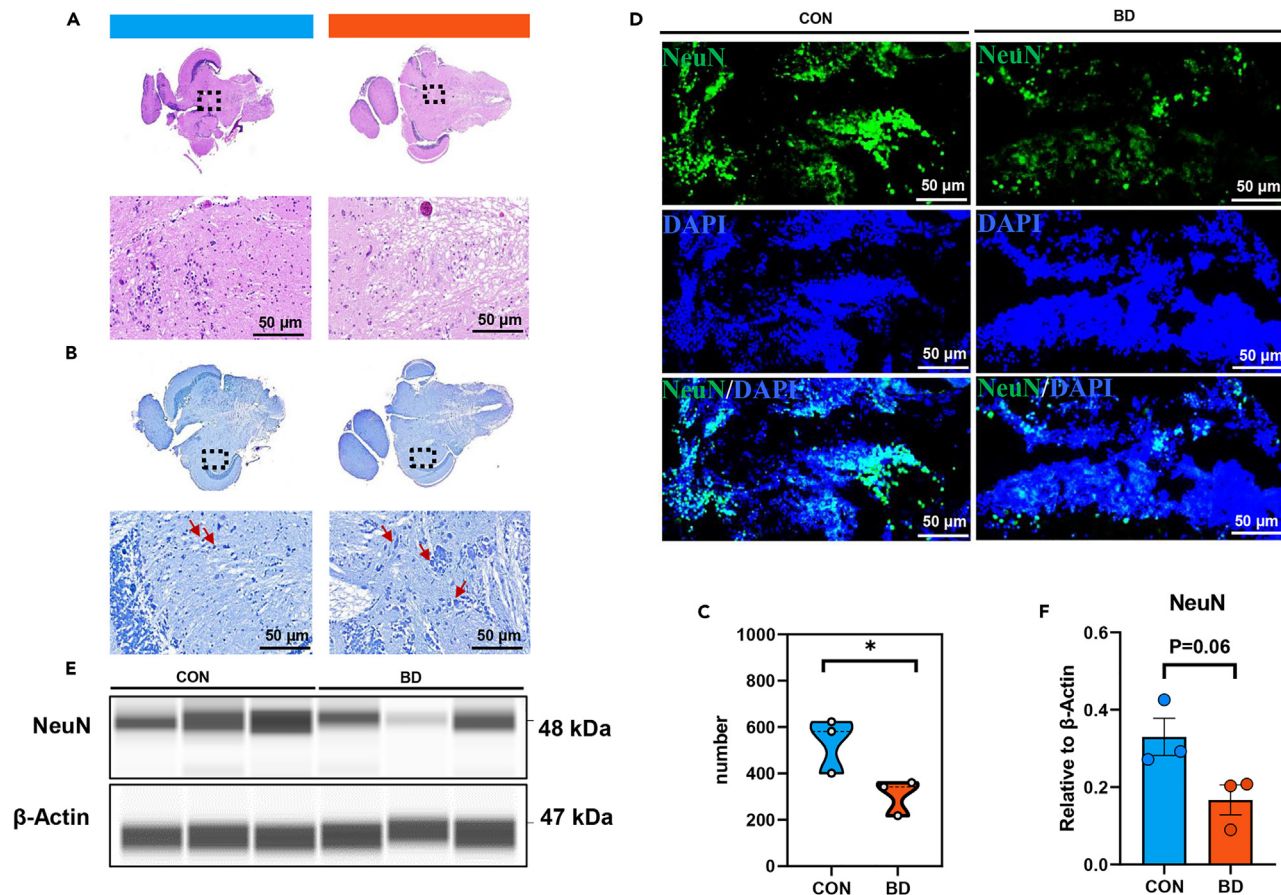


Figure 2. Histopathological characteristics of BD zebrafish

(A and B) Histomorphometric analysis of midbrain from CON (n = 3) and BD zebrafish (n = 3) stained with H&E, scale bar = 50 μ m (A); Nissl staining was used to mark Nissl bodies in neurons (B). Red arrow, cytosolic swelling, scale bar = 50 μ m.

(C) Total number of Nissl-positive neurons in per field was quantified with ImageJ.

(D) Representative immunofluorescence images of midbrain after staining for NeuN (neurons, green) and DAPI (all nuclei, blue). Scale bar = 50 μ m.

(E and F) Expression of NeuN in CON and BD was detected by Western blot. Data are shown as mean \pm SEM, *p < 0.05.

significantly downregulated (Figure 3B). Principal component analysis showed a clear difference between BD and controls in the metabolomic, lipidomic, and transcriptomic datasets (Figure 3C).

Integrative omics reveals impaired neurotransmission in BD

In revealing the holistic molecular consequences and identifying the key affected pathways linked with the observed phenotypes, an integrated multi-omic technique was used. Integrated molecular pathway-level analysis facilitates the identification of key dysregulated pathways. The differentially molecular metabolomic–lipidomic–transcriptomic screen was significantly enriched in biological processes, including amino acid metabolism, lipid metabolism, nervous system, and intracellular signaling pathways (Figure 3D), indicating a global dysregulation in neurotransmission. A summary of the major metabolic changes was plotted on a metabolic network map (Figure 3E), showing consistent alterations in key metabolites or lipids and their associated transcripts.

In amino metabolism, we performed multi-omic integration analysis mapping to the KEGG databases to facilitate analysis of these metabolites and transcript results that were significantly associated with BD. The results further highlighted a significant (FDR < 0.05) over-representation of pathways associated with tryptophan, tyrosine, phenylalanine, arginine, proline, and glutamate metabolism (Figure 3D). In addition, metabolites and associated transcripts were significantly enriched in the nervous system, including dopaminergic, serotonergic, glutamatergic, cholinergic, and GABAergic synapse (Figure 3D), predominantly associated with synaptic transmission in the brain.

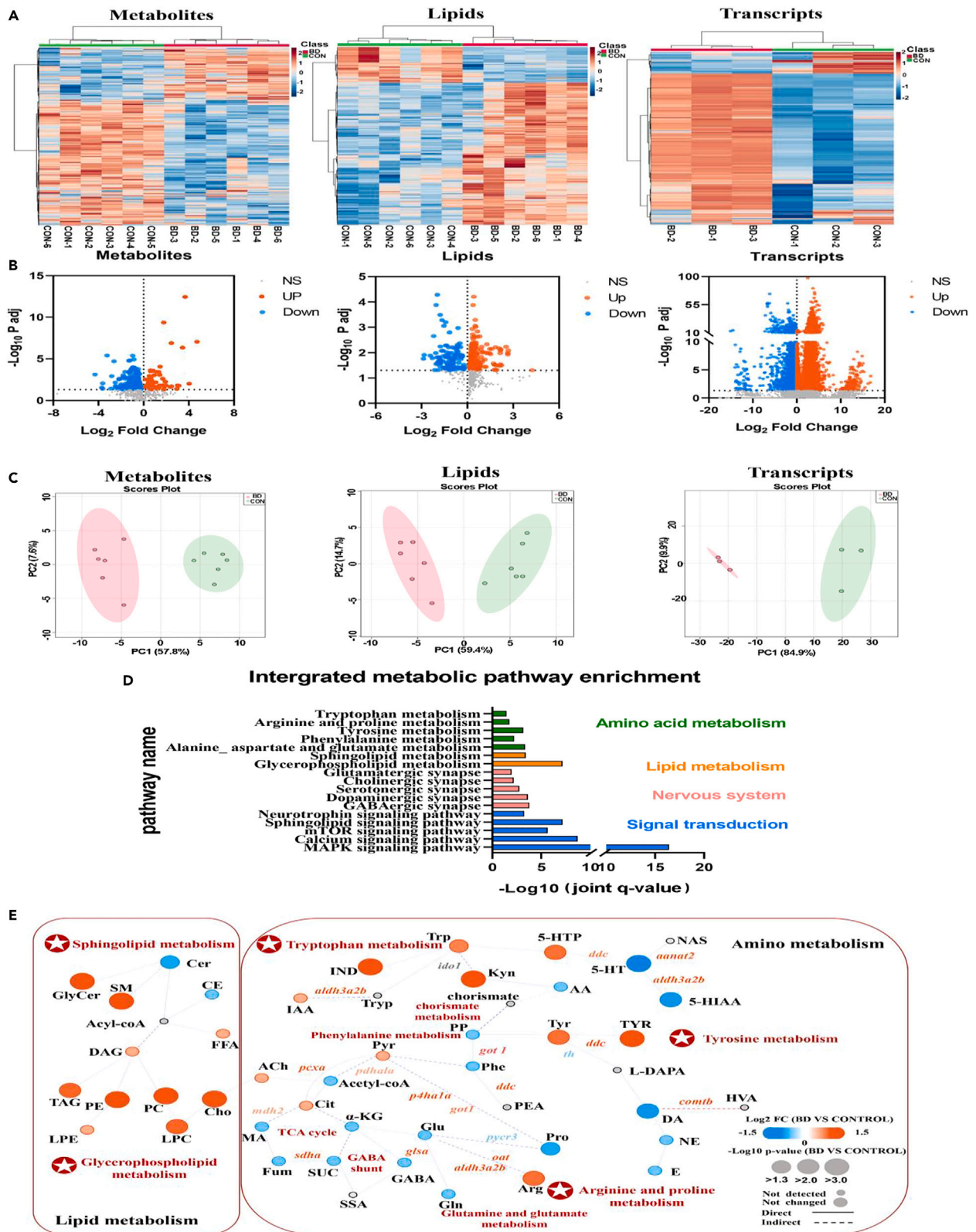


Figure 3. Multi-omic molecular profile of BD zebrafish

(A) Hierarchical clustering analysis of metabolites, lipids and genes in brain tissues of CON and BD zebrafish.
 (B) Volcano plots for metabolomic, lipidomic and transcriptomic analysis in BD brain tissue. FDR < 0.05 and fold change > 1 were defined as significantly upregulated molecules; FDR < 0.05 and fold change < 1 were defined as significantly downregulated molecules. Red dots indicate significantly upregulated molecules; blue dots indicate significantly downregulated molecules, and black dots indicate non-significantly different molecules.
 (C) Principal component analysis plots of all 661 metabolites, 643 lipids and 32057 transcripts clearly separate the profiles of BD from controls.
 (D) Significant enrichment pathways identified by integrated molecular pathway-level analysis, integrating metabolites, lipids and transcripts (FDR < 0.05). The enrichment pathways were categorized as follows: amino acids (green), lipids (orange), nervous system (pink), and signal transduction (blue).
 (E) Integrated network analysis combining multi-omic molecules using MetaboAnalyst and IMPaLA platform. Each node (circle) represents a metabolite or lipid (CON and BD, n = 6), and each edge connecting the nodes represents a transcript (CON and BD, n = 3) encoding an enzyme based on a biochemical relationship. Solid or dashed connecting lines represent biochemical reactions that occur directly or indirectly. The size of each node reflects their p value. The shade of color represents the degree of relative change (blue indicates a decrease; red indicates an increase; gray indicates not detected).

These findings were validated by performing HPLC-MS/MS-based targeted metabolic analysis of brain tissues. Consistent with the untargeted metabolomic result, two major neuroactive metabolic pathways, namely, the aromatic amino acid pathways (tyrosine and tryptophan metabolism) and amino acid pathways (arginine and proline metabolism), were worthy of examination (Figure 3E). A number of neurotransmitters were significantly altered in the BD group, spanning amino acid neurotransmitter glycine (Figure 4A), monoamine neurotransmitters, including dopamine and serotonin (Figure 4B). We also explored the association between metabolomic and genomic features to identify the potential genomic drivers contributing to the formation of metabolomic features. We observed that tyrosine and tryptophan metabolism was significantly altered, as demonstrated by the downregulation of monoamine neurotransmitters (dopamine and serotonin) and 5-HIAA (serotonin derivatives; Figures 3E, 4B, and 4D), as well as increased levels of their precursors (tyrosine and tryptophan), intermediates (5-hydroxy-L-tryptophan, kynurenate, tyramine, and indole; Figures 3E, 4C, and 4D) and their associated genes (*aox5*, *aldh3a2b*, *ddc*, *aanat2*, *got1*, *th*, *comtb*, and *tyrp1b*) (Figures 3E and 4F). In addition to changes in aromatic amino acid pathways, arginine and proline metabolism was also enhanced in BD, as characterized by nine genes (*got1*, *p4ha1a*, *dao.3*, *amd1*, *aldh3a2b*, *oat*, *ckma*, *pycr3*, and *arg1*) associated with neurotransmitters, which have been shown to be altered (Figures 3E and 4F), and two metabolites (arginine and proline) along with changes in the levels of several neuromodulators and neurotransmitters (Figures 3E, 4E, S6A, and S6B). These results indicated that the neuroactive metabolite production system was severely blocked.

In addition to changes in amino metabolism, significantly enriched pathways also highlighted some lipid metabolism pathways in BD. Integrated transcriptomic and lipidomic analyses demonstrated that significantly altered lipids and genes were primarily enriched in sphingolipid metabolism and glycerophospholipid metabolism (Figure 3D). Based on the abundance of lipids, we observed a slight upward trend in free fatty acids (FFA) in the BD group compared with the controls (Figure S6C). After entering the cells, FFA are converted to acyl coenzyme A (acyl-CoA), and then they enter the sphingolipid synthesis pathway to form ceramides (Cer), which was severely reduced. Meanwhile, two lipid subclasses (glycosylceramides [GlyCer] and sphingomyelins [SM]) involved in sphingolipid metabolism were elevated (Figures 4G and S6D), along with 15 genes (*asah2*, *sgpl*, *cerk*, *neu1*, *plpp3*, *smpd3*, *cers4b*, *cers1*, *galca*, *acer2*, *kdsr*, *ppap2d*, *sgpp2*, *smpd2a*, and *cers2a*) linked with the sphingolipid metabolism pathway (Figure 4I). This result indicated a defect in the conversion of FFA to Cer and a depletion of their further metabolism to SM and GlyCer. Moreover, the majority of lipids (phosphatidylcholines [PC], phosphatidylethanolamines [PE] and lyso-phosphatidylcholines [LPC]) in glycerophospholipid metabolism were elevated in the BD group (Figures 4H and S6E), which is consistent with the remarkable upward trend in 14 genes (*pgs1*, *agpat5*, *si:ch73-21k16.1*, *plpp3*, *cds1*, *si:ch73-55i23.1*, *pld2*, *gnpat*, *gpam*, *gpd11*, *pcyt1ba*, *ppap2d*, *lpin2*, and *lypla2*) involved in glycerophospholipid metabolism (Figure 4I). These findings indicated that sphingolipids and glycerophospholipids, the major lipid components of cell membranes, were severely disrupted.

Collectively, these results indicated that the pathophysiology in this drug-induced model of BD induces alterations in neurotransmitter metabolic pathways which may limit the synthesis of the neurotransmitters (serotonin, dopamine, and glycine) and impair their involvement in synaptic transmission. These changes, combined with imbalances in membrane lipid metabolism, indicated a disruption in neuronal membrane structure, thereby leading to a comprehensive disturbance of interneuronal signaling. These perturbations may lead to the development of neuronal synaptic transmission dysfunction.

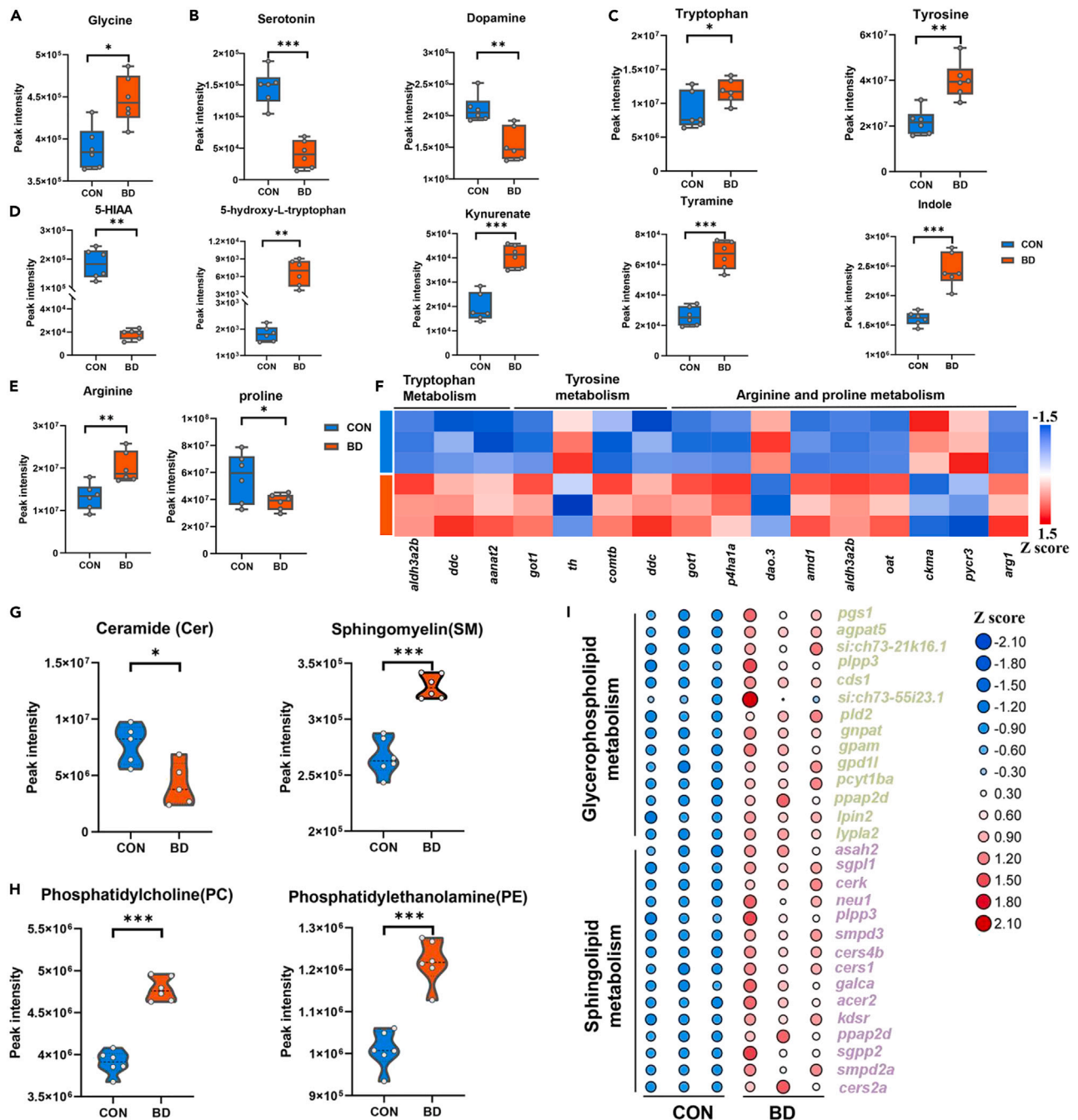


Figure 4. Dysregulated neurotransmission in BD zebrafish

(A–E) Box and Whisker plots of brain amino acid neurotransmitter glycine (A), monoamine neurotransmitters dopamine and serotonin (B), aromatic amino acids tyrosine and tryptophan (C), related metabolites involved in tryptophan metabolism (D), and amino acids arginine and proline (E). * $p < 0.05$, *** $p < 0.01$, **** $p < 0.001$, unpaired two-tailed Student's t test or the Wilcoxon Rank-Sum Test.

(F) Heatmap shows overall changes in genes related to amino acid metabolism regulating neurotransmission.

(G and H) Violin plot of brain sphingolipid Cer and SM (G) and glycerophospholipid PC and PE (H). Cer, ceramides; SM, sphingomyelins; PC, phosphatidylcholines; PE, phosphatidylethanolamines. Data are shown as mean \pm SEM, * $p < 0.05$, ** $p < 0.01$, **** $p < 0.001$, unpaired two-tailed Student's t test.

(I) Heatmap shows overall changes in genes related to lipid metabolism regulating neurotransmission (CON and BD, $n = 6$) and genes (CON and BD, $n = 3$).

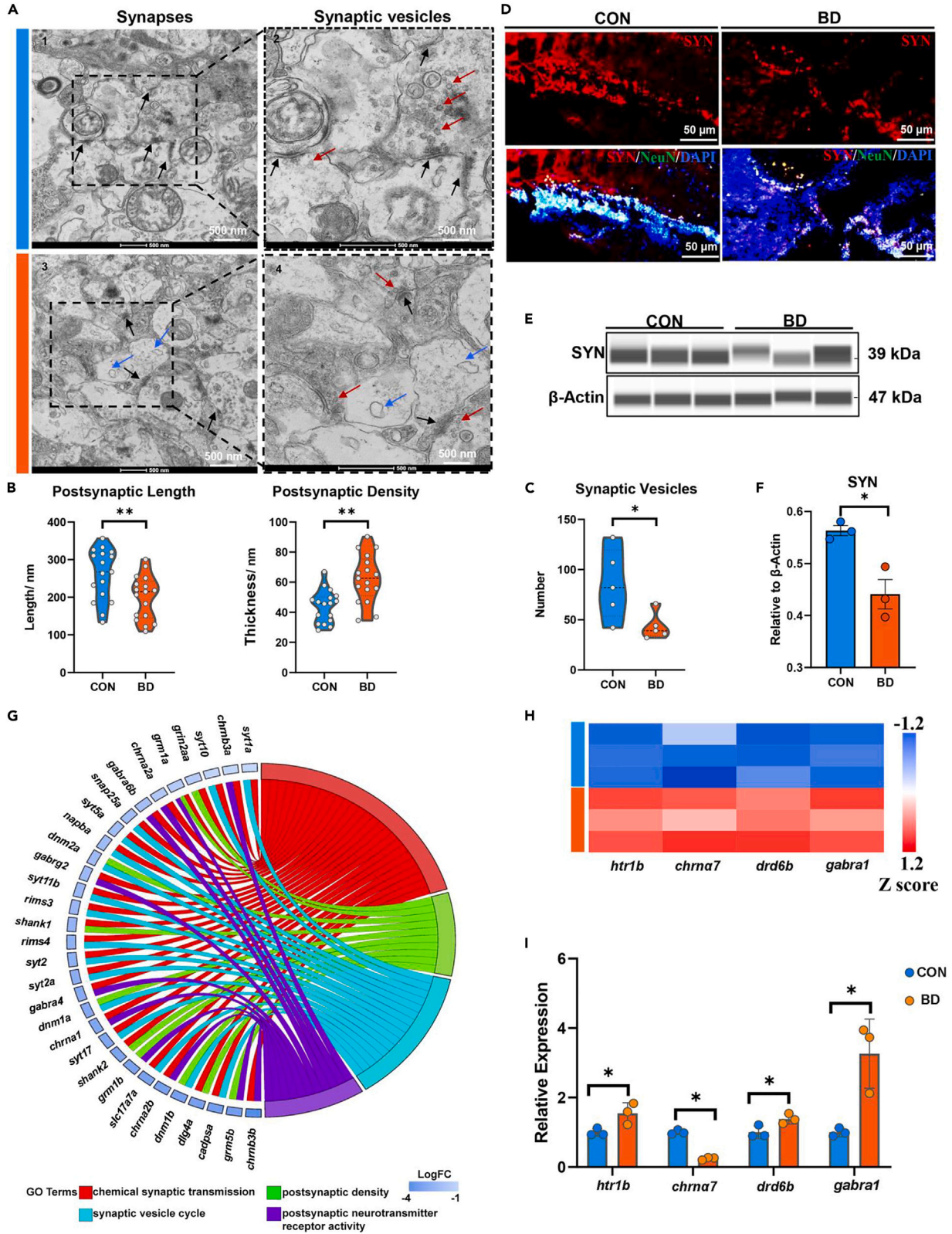


Figure 5. Synaptic damage in BD zebrafish

(A) Representative electron synapses of midbrain from control and BD zebrafish (CON and BD, n = 3). Each image represents one individual subject (scale bar = 500 nm). (Black arrow, synapse; red arrow, synaptic vesicle; blue arrow, vacuolation.).

(B and C) Quantitative measurements postsynaptic length, postsynaptic density (B) and synaptic vesicles (C) using ImageJ. 17 randomly selected fields of view from each sample were used to determine postsynaptic length and postsynaptic density; six randomly selected fields of view from each sample were used to determine synaptic vesicles. * $p < 0.05$, ** $p < 0.01$, unpaired two-tailed Student's t test.

(D) Representative immunofluorescence images of midbrain after staining for SYN (synaptophysin, red), NeuN (neurons, green) and DAPI (all nuclei, blue). Scale bar = 50 μm .

(E and F) Expression of SYN in CON and BD was detected by Western blot. * $p < 0.05$, unpaired two-tailed Student's t test, data are shown as mean \pm SEM.

(G) Chord plot representation of 31 differentially expressed genes (FDR < 0.05) from four enriched pathways generated by the bioinformatic platform. The color map represents fold change (FC) of genes (\log_2 FC) and enriched pathways (chemical synaptic transmission, red; synaptic vesicle cycle, blue; postsynaptic density, green; postsynaptic neurotransmitter receptor activity, purple).

(H and I) Quantitative analysis of genes regulating neurotransmitter receptor activity using transcriptome sequencing (H) and qPCR (I). *chrna7* related to cholinergic receptors; *Htr1b* related to serotonin receptors; *drd5b* related to dopamine receptors and *gabra1* related to GABA receptors. * $p < 0.05$, unpaired two-tailed Student's t test, data are shown as mean \pm SEM.

BD model is associated with impaired synaptic ultrastructure and synaptic transmission

Next, we explored the association of the aforementioned metabolic alterations with alterations in neuronal morphology and function. Under TEM, the neurons of the control group displayed an intact structure with normal synaptic structures and distinct boundaries among organelles within the cytoplasm (Figure 5A). Compared with the controls, the BD zebrafish showed reduced intracellular organelles, loss of structural integrity, and profound disruption of synaptic ultrastructure in the neurons, in which the length of the postsynaptic densities was decreased with the increase of thickness (Figure 5A). In addition, the quantification of the length and thickness of PSD confirmed the significant alteration of synaptic ultrastructure (Figure 5B). Moreover, morphometric analyses exhibited a significant reduction in synaptic vesicle, whereas the number of synapses remained unaffected in BD (Figures 5C and S7A). Consistent with the reduced number of synaptic vesicles, immunofluorescence and Western blot results revealed a marked reduction in synaptic vesicle marker synaptophysin, indicating that the synaptic ultrastructure was remodeled in the BD group (Figures 5D, 5E, and 5F). These morphological alterations were associated with the downregulation of essential genes regulating synaptic vesicle cycle, PSD, and synaptic transmission (Figure 5G).

Determining whether these abnormalities in synaptic morphology resulted in synaptic dysfunction in specific neurons may contribute to the pathogenesis of BD. Through integrated molecular pathway enrichment analysis, we observed that glutamatergic, cholinergic, serotonergic, dopaminergic, and γ -aminobutyric acid (GABA) synapse, which were predominantly associated with synaptic transmission, were significantly enriched (Figure 3D). In confirming this finding, we quantified key genes for neurotransmitter receptors on the postsynaptic membrane that regulates synaptic transmission by transcriptome sequencing and qPCR and found significant activation or inhibition of neurotransmitter receptor activity in the BD group, characterized by the downregulation of cholinergic receptors (*chrna7*) along with the upregulation of serotonin receptors (*htr1b*), dopamine (DA) receptors (*drd5b*), and GABA receptors (*gabra1*; Figures 5H, 5I, S7B, and S7C). Collectively, these results underscore the importance of synaptic ultrastructural remodeling in a drug-induced model of BD, which was characterized by affecting pre- and postsynaptic determinants of synaptic transmission, including synaptic vesicle cycle and PSD, thereby interfering with neurotransmitter release and neurotransmitter receptor responses and leading to synaptic dysfunction and impaired neurotransmission.

Synaptic damage in a model of BD is associated with MAPK/JNK-mediated neuroinflammation

We investigated the intracellular signal transduction cascade response in BD zebrafish to investigate the mechanisms for BD synaptic structure damage and dysfunction. Integrated molecular pathway-level analysis identified five dysregulated signal transduction pathways, including neurotrophin, sphingolipid, mTOR, calcium, and MAPK signaling pathway, with the MAPK signaling pathway as the most prominent (Figure 3D). We performed qPCR to validate the RNA-seq results, which confirmed the upregulation of MAPK cascade-related genes (Figures 6A and 6B), and the significantly altered genes were primarily associated with the MAPK/c-Jun N-terminal kinase (JNK) signaling pathway. Similarly, the significant increase in the *p*-JNK/JNK ratio in Western blotting analysis also indicates the activation of JNK (Figures 6C, 6D, and S8A), all of which implied that an MAPK/JNK intracellular signaling cascade was initiated in BD zebrafish.

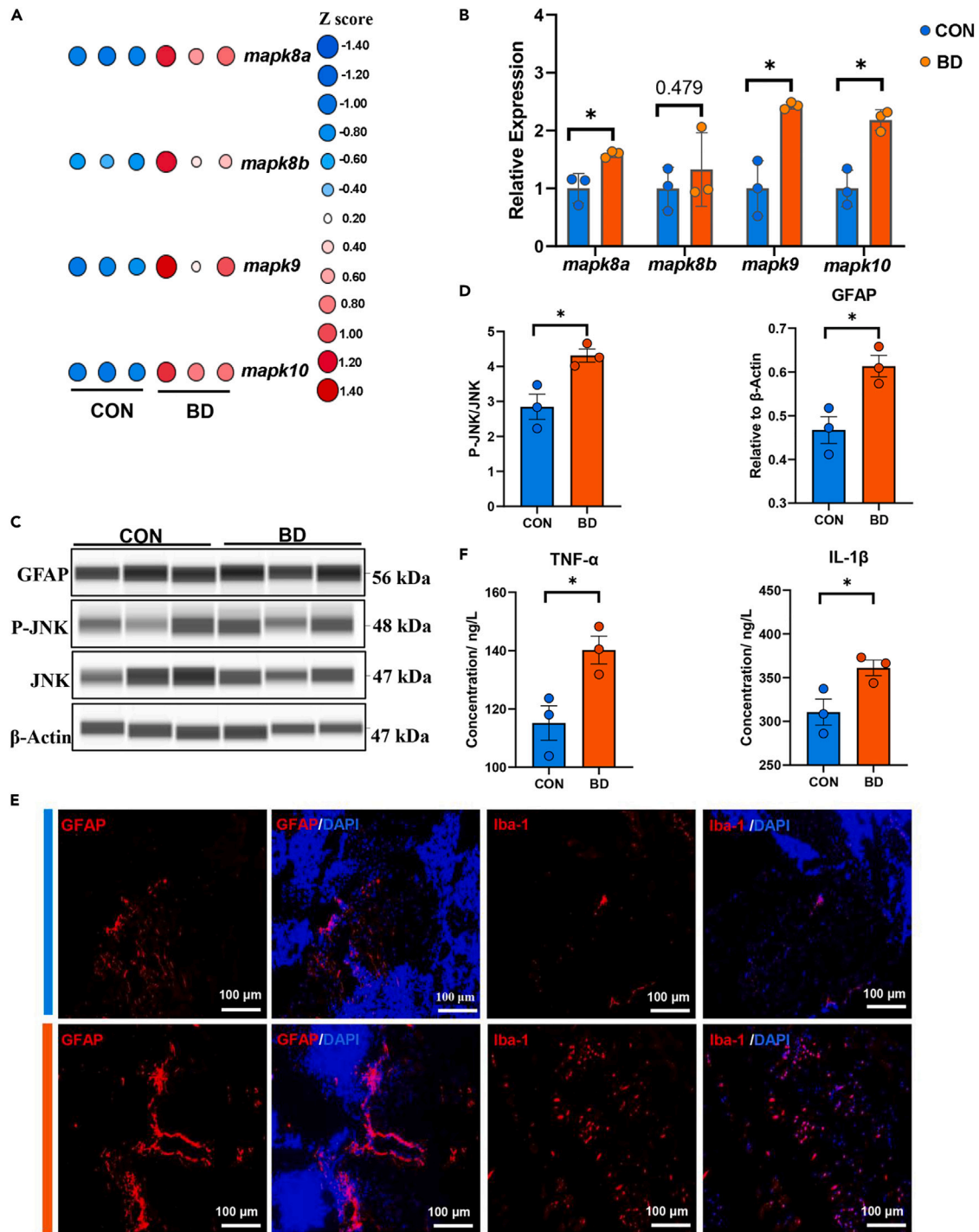


Figure 6. MAPK/JNK-mediated neuroinflammation in BD zebrafish

(A) Heatmap shows overall changes in genes related to the MAPK/JNK signaling pathway.

(B) Quantitative analysis of genes related to the MAPK/JNK signaling pathway using qPCR.

(C and D) Expression of GFAP, P-JNK and JNK in CON and BD was detected by Western blot. * $p < 0.05$, unpaired two-tailed Student's *t* test, data are shown as mean \pm SEM.

(E) Representative immunofluorescence images of midbrain after staining for GFAP (astrocyte, red), Iba-1 (microglia, red), NeuN (neurons, green), and DAPI (all nuclei, blue). Scale bar = 100 μ m.

(F) Quantitative analysis of pro-inflammatory cytokine levels using ELISA. * $p < 0.05$, unpaired two-tailed Student's *t* test, data are shown as mean \pm SEM (CON and BD, $n = 3$).

Furthermore, we determined whether the activation of the MAPK/JNK signaling pathway was accompanied by neuroinflammation and neuronal apoptosis, thereby contributing to the pathogenesis of a model of BD. Consistent with our finding of the activation of the MAPK/JNK signaling pathway, we found resident immune cells (microglia and astrocytes) in an activated state by measuring astrocyte-specific antibodies (GFAP) and microglia-specific antibodies (Iba-1) levels (Figures 6C, 6D, and 6E). In confirming these results, we measured the levels of pro-inflammatory cytokines secreted by immune cells and showed that the production of TNF- α and IL-1 β were consistently higher in BD than in controls, whereas no significant change in IL-6 production was observed (Figures 6F and S8B). Collectively, these results indicated that activated microglia and astrocytes, which released high levels of IL-1 β and TNF- α , mediate the MAPK/JNK inflammatory signaling cascade response and further trigger neuroinflammation, which may be related to the synaptic pathology that we observed in our model of BD.

DISCUSSION

Despite accumulating studies showed pathophysiological and metabolic remodeling in BD,³⁷ the underlying mechanism remains unresolved, particularly in vertebrate models. Here, we present an in-depth multi-omic characterization of BD zebrafish combined with analysis of synaptic ultrastructure and function. To our knowledge, this is the first time that a zebrafish vertebrate model has been used to reveal the molecular mechanisms underlying potentially relevant pathophysiology in a BD model, including metabolic derangements of the major biochemical pathways involved in neurotransmission. These mechanisms were related with the accumulation of damaged synapse, and the development of JNK-mediated neuroinflammation because of the combination of failure to synaptic vesicle cycle, remodeling of the PSD and increased TNF- α and IL-1 β .

Previous reports have used rodent behavior to model BD, and they have focused only on either the manic or depressive poles.³⁶ However, an ideal animal model of BD is characterized by cyclic episodes of depression and hypomania/mania.³⁸ In individuals with BD, manic episodes include hyperactivity, euphoria, hypersexuality, and psychosis. Conversely, depressive episodes involve other manifestations, such as decreased energy, social withdrawal, and psychomotor retardation.³⁹ In zebrafish, novel tank test (NTT) was used to assess the influence of external factors on the behavioral activity of zebrafish.⁴⁰ In this case, aquatic animals are often inclined to explore the primary peripheral zones. Location preference is a reliable indicator for assessing anxiety- and depression-related behavior. In addition, the Noldus software can further analyze the tracking videos obtained through the NTT to quantify the indicators of behavioral phenotypes associated with BD.²⁵ Here, we observed a decrease in total exploration time and frequency and an increase in manic, hyperactivity, and wall-hugging behavior characterizing depressive/manic in the model group of zebrafish in NTT. Compared to BD rodent models,³⁵ our constructed BD zebrafish model was more sensitive to behavioral phenotypes that were closely related to BD, which covered both depressive-like and manic-like behaviors. Our data supported the analysis of potential molecular features associated with BD pathogenesis in zebrafish.

We gained a “multi-omic landscape” view of these metabolites through chemical and pathway enrichment analyses. Compared with controls, we noted that the highly enriched metabolites in BD zebrafish brain were clustered in tryptophan, tyrosine, arginine, and proline metabolism pathways. Consistent with previous studies,⁴¹ perturbations in the metabolic pathways of aromatic amino acids, particularly tryptophan and tyrosine, may contribute to diverse psychiatric and behavioral disorders, including anxiety,⁴² schizophrenia,⁴³ and depression,⁴⁴ based on the facts that tryptophan is the precursor for serotonin and tyrosine is the precursor for dopamine.⁴⁵ Our results indicated that monoamine neurotransmitters including serotonin and dopamine were involved in a model of BD and that their reduced production manifested the manic and depressive behavior in BD zebrafish. The important role of dopamine and serotonin changes in emotion regulation has been reported previously,⁴⁶ but the underlying mechanism remains unclear. We determined that the low production of serotonin was due to shunting of tryptophan from the serotonin pathway to kynurenine (KYN) and aromatic hydrocarbon receptor (AhR) pathway. In general, tryptophan metabolism constitutes primarily three branches, including the AhR pathway, KYN pathway, and serotonin pathway.⁴⁷ The KYN pathway contains many immunoreactive and neuroactive intermediate metabolites, which produce neuroprotective (kynurenic acid) and neurotoxic (quinolinic acid) metabolites.⁴⁸ In addition, considerable evidence suggests that alterations in the balance among these neuroactive KYN pathway metabolites contribute to neurodegenerative and neuropsychiatric diseases.^{49,50} Remarkably, pro-inflammatory cytokines (e.g., interferon and TNF- α) have been shown to mediate IDO enzymatic activity, resulting in an excess of metabolites with specific neuroactive properties in the KYN pathway, which is thought to be

responsible for a variety of neuropsychiatric disorders.⁴⁸ This result was consistent with the elevated levels of pro-inflammatory cytokines (TNF- α and IL-1 β) and KYN in the BD zebrafish brain in our study. However, the reason why inflammatory cytokines upregulated in response to IDO1 induction and accumulation of KYN remains unclear. Here, we found that activation of the JNK inflammatory pathway was highly correlated with the KYN pathway. In addition, Indole, as microbiota-derived tryptophan metabolite, which is ligands for AhR, can sense xenobiotic stimulation, and it has been implicated in pathogenesis of inflammatory bowel disease⁵¹ and mood disorders.⁵² In our study, the decrease of serotonin in the BD zebrafish brain was also accompanied by an increase in indole, indicating that tryptophan was shunted away from the serotonin pathway and into the AhR pathway. Our result complement previous research⁵³ that commensal microbiota in the gut can mediate inflammatory CNS reactions through direct humoral pathways featuring decreased serotonin and enriched indole.

In addition to tryptophan metabolism, tyrosine, proline, and arginine metabolism were also found to be enriched. Therefore, these pathways are involved in neurotransmission as well. Tyrosine is the precursor for dopamine and tyramine.⁵⁴ Here, in the case of tyramine production pathway overactivation, tyrosine was massively diverted to tyramine production, causing a deficiency in dopamine, an important regulator of mood, and this finding explained the BD-like behavior that we observed in BD zebrafish. In line with our finding, previous study has shown that dopamine neurons regulate the neural encoding and expression of depression-related behavior in mice,⁵⁵ a finding that not only underlined the role of dopamine in emotion regulation but also validated our experimental results. In addition, the excitatory neurotransmitter glutamate is the precursor of arginine and proline, and it represents the end product of the degradation of proline and arginine. Glutamate is linked to the catabolic processes of arginine and proline through GABA shunt and the tricarboxylic acid (TCA) cycle associated with the mitochondria.⁵⁶ Notably, we found that the imbalance in proline and arginine metabolism in the BD zebrafish brain was caused by reduced levels of circulating glutamate, due to mitochondrial dysfunction and energy metabolism imbalance (Figure S6F). Our findings provided critical insights into the previously reported role of mitochondrial dysfunction in the pathogenesis of BD.⁵⁷ Interestingly, proline showed different trends in BD zebrafish and depressed mice,⁵⁶ which indicated that proline is a potential biomarker when differentiating BD from depression or because of differences in the species studied. These results highlight the potential role of proline metabolism in affective psychosis. Collectively, these results indicated that disturbed amino acid metabolism greatly contributes in a model of BD by modulating neurotransmitter metabolic pathways.

In addition to altered amino acid metabolism that limits neurotransmission in BD, we found that lipid metabolism was dysregulated in BD zebrafish. Lipids play a key role in neuronal function, and disturbances in the lipid composition of the brain may reflect alterations in perception and emotional behavior, which plays an essential role in the pathological mechanism of neuropsychiatric disorders.^{36,58} In particular, dysfunction of SM has been identified as a crucial pathogenetic pathway of MDD³⁶ and anxiety,⁵⁹ but its biological role in these disorders remains unclear. Here, we observed that alterations in sphingolipid and glycerophospholipid metabolism were prominent features of BD zebrafish. The majority of metabolites involved in sphingolipid (Glycer, SM, Cer) and glycerophospholipid (PE, PC, LPC) metabolism were enriched, but Cers involving the sphingolipid metabolism were depleted in BD zebrafish relative to controls. Sphingolipids together with glycerophospholipids and cholesterol are the most abundant lipids in brain membranes, and are associated with transmembrane signaling.⁶⁰ Sphingomyelins play a key role in electrical insulation of axons and axon extension,⁶¹ while PE, PC, and LPC are key lipids for maintaining the structural integrity and self-regulation of neuronal membranes.⁶² Notably, the integrity of cell membranes and signaling through them depends on the lipid homeostasis in the brain. Hence, these findings verified that membrane damage and Impaired synaptic transmission caused by imbalances in sphingolipid and glycerophospholipid metabolism played an important role in BD-like zebrafish. Combined with alterations in amino acid metabolism and neurotransmitter receptors (*chrna7*, *htr1b*, *drd5b*, *gabra1*) activity, our study showed that the disruption of lipid membrane structures affects synaptic transmission processes, including synaptic vesicle cycle and protein receptor-mediated intracellular signaling pathways. Consistent with these findings, our pathological and TEM ultrastructural results also confirm the loss of structural integrity of neuronal membranes, remodeling of PSD, and reduction of synaptic vesicles in BD zebrafish. Collectively, these data demonstrated that disturbances in sphingolipid and glycerophospholipid metabolism contribute to BD by perturbing synaptic membrane structure and neurotransmitter receptors activity.

Accumulating data support the hypothesis that neuroinflammation contributes to the progression of synaptic dysfunction.⁶³ In neurodegenerative diseases, neuroinflammation accompanied by synaptic

dysfunction is a common pathological feature in the early stages of these diseases, such as Alzheimer's disease⁶⁴ and Parkinson's disease.⁶⁵ Notably, we observed that activated microglia and astrocyte in BD zebrafish released high levels of pro-inflammatory factors IL-1 β and TNF- α , which activated MAPK/JNK signaling pathway-mediated neuroinflammation. These findings indicated that MAPK/JNK inflammatory cascade contributed to the synaptic pathology that we observed in BD. JNK and p38 MAPK, which are two branches of the MAPK signaling pathway, can be activated by various environmental stresses and pro-inflammatory cytokines (e.g. TNF- α , IL-1 β , and IL-6), are involved in stress responses such as inflammation and apoptosis.⁶⁶ Previous studies reported that p38 MAPK altered neuronal plasticity and the efficacy of synaptic transmission in AD mouse models.⁶⁷ Meanwhile, blockade of P38 MAPK normalized GABA synaptic transmission and reversed anxiety-like behavior in chronically alcohol-exposed mice.⁶⁸ Collectively, these data underscored the importance of MAPK-mediated inflammatory responses on synaptic dysfunction. In contrast to these results, our data showed a crucial mechanism by which JNK inflammatory cascade contributed to the outcome of serotonergic and dopaminergic synaptic dysfunction in BD, rather than MAPK p38 (Figures S9A, S9B, and S9C). These discrepancies might be due to the use of animals with different species, disease models, and methods of inducing neuroinflammation. Collectively, JNK-mediated neuroinflammation induced different degrees of dysfunction of synaptic transmission at serotonergic and dopaminergic synapses associated with emotion regulation in BD zebrafish.

Limitations of the study

This is the first study to introduce a drug-induced zebrafish model of BD. At the same time, behavioral-histopathological visualization techniques and high-coverage metabolomic, lipidomic, and transcriptomic analyses were employed, which allowed complete profiling and mining of the specific molecular signatures of BD zebrafish, thus providing critical biological insights into the pathogenesis of BD. We also noted some caveats and limitations of the present study. Firstly, the simultaneous observation of mania and depressive behavior in our model, which differs between BD in human and this zebrafish model, and therefore future studies are required for development of alternative approaches to better mimic BD in zebrafish. Secondly, although we performed behavioral analysis and validation of zebrafish model of BD we constructed, this did not fully evaluate alternating episodes of mania and depression and some of the associated manifestations such as euphoria, increased self-esteem, irritability, persistent sadness, and anhedonia. As such, we encourage future research on methods for assessing BD-like behaviors. Thirdly, we only observed the molecular characteristics of female BD zebrafish; but these results may vary by gender. Thus, more in-depth analysis is anticipated to deepen our knowledge on the molecular mechanism of gender-specific characteristics in the future. Fourthly, based on the findings of this study, further pathway-specific interventions could be done on zebrafish or other biological models to enhance our understanding of the pathogenesis and progression of BD. Finally, in addition to brain, the antibiotic ciprofloxacin also has potential toxicity on organs such as the intestine and heart. It is expected that future research will further analyze the bidirectional interaction between the nervous and gastrointestinal systems in the zebrafish model of BD based on the communication system of microbiome-gut-brain axis.

STAR★METHODS

Detailed methods are provided in the online version of this paper and include the following:

- KEY RESOURCES TABLE
- RESOURCE AVAILABILITY
 - Lead contact
 - Materials availability
 - Data and code availability
- EXPERIMENTAL MODEL AND SUBJECT DETAILS
- METHOD DETAILS
 - Behavioral assay
 - Histological assessments
 - RNA-seq analysis from brain samples
 - Untargeted metabolomic analysis
 - Untargeted lipidomic analysis
 - Targeted metabolomic analysis
 - Transmission electron microscopy (TEM)
 - Quantitative real-time PCR (qPCR) analysis

- Immunostaining of brain sections
- Western blotting
- Enzyme-linked immunosorbent assay (ELISA)
- **QUANTIFICATION AND STATISTICAL ANALYSIS**
- mRNA-seq analysis
- Untargeted metabolomic and lipidomic analysis
- Targeted metabolomic analysis
- Integrated analysis using metabolites, lipids and transcripts
- Statistical analysis

SUPPLEMENTAL INFORMATION

Supplemental information can be found online at <https://doi.org/10.1016/j.isci.2023.106744>.

ACKNOWLEDGMENTS

This work was supported by National Key Research and Development Program of China (2018YFC1603000) and Science and Technology Innovation Program of the Chinese Academy of Agricultural Sciences (CAAS-ASTIP-IQSTAP). In addition, the work was supported by instrumentation and technical support from Waters company (Waters, USA).

AUTHOR CONTRIBUTIONS

Y.L., Y.Q., and J.Q. were involved in the design of the experiments, data analysis, and writing the first draft of the manuscript. M.M., L.H., X.Z., and Z. L., performed the brain tissue collection. Y.L., L.Z., and Y.P. performed data acquisition. Y.L. and L.Z. curated the MS spectra. T.W., Y.Q., and J.Q. carried out data normalizations. X.M., J.Q., and Y.Q. assessed the quality of figures. J.Q. and Y.Q. supervised the study and secure funding. All authors subsequently took part in the revision process.

DECLARATION OF INTERESTS

The authors declare no competing interests.

INCLUSION AND DIVERSITY

We support inclusive, diverse, and equitable conduct of research.

Received: January 10, 2023

Revised: March 16, 2023

Accepted: April 21, 2023

Published: April 25, 2023

REFERENCES

1. Dong, X., Liao, Z., Gritsch, D., Hadzhiev, Y., Bai, Y., Locascio, J.J., Guennewig, B., Liu, G., Blauwendraat, C., Wang, T., et al. (2019). Enhancers active in dopamine neurons are a primary link between genetic variation and neuropsychiatric disease (vol 21, pg 1482, 2018). *Nat. Neurosci.* 22, 144–147. <https://doi.org/10.1038/s41593-018-0277-z>.
2. DE, B. (2013). Diagnostic and Statistical Manual of Mental Disorders. DSM. <https://doi.org/10.1590/s2317-17822013000200017>.
3. Brenner, C.J., and Shyn, S.I. (2014). Diagnosis and management of bipolar disorder in primary care A DSM-5 update. *Med. Clin.* 98, 1025–1048. <https://doi.org/10.1016/j.mcna.2014.06.004>.
4. Scott, J., Kallestad, H., Vedaa, O., Sivertsen, B., and Etain, B. (2021). Sleep disturbances and first onset of major mental disorders in adolescence and early adulthood: a systematic review and meta-analysis. *Sleep Med. Rev.* 57, 101429. <https://doi.org/10.1016/j.smrv.2021.101429>.
5. Arnold, L.M. (2003). Gender differences in bipolar disorder. *Psychiatr. Clin.* 26, 595–620. [https://doi.org/10.1016/s0193-953x\(03\)00036-4](https://doi.org/10.1016/s0193-953x(03)00036-4).
6. Marrie, R.A., Hitchon, C.A., Walld, R., Patten, S.B., Bolton, J.M., Sareen, J., Walker, J.R., Singer, A., Lix, L.M., El-Gabalawy, R., et al. (2018). Increased burden of psychiatric disorders in rheumatoid arthritis. *Arthritis Care Res.* 70, 970–978. <https://doi.org/10.1002/acr.23539>.
7. Vahratian, A., Blumberg, S.J., Terlizzi, E.P., and Schiller, J.S. (2021). Symptoms of anxiety or depressive disorder and use of mental health care among adults during the COVID-19 pandemic - United States, august 2020-february 2021. *MMWR Morb. Mortal. Wkly. Rep.* 70, 490–494. <https://doi.org/10.15585/mmwr.mm7013e2>.
8. Karantonis, J.A., Rossell, S.L., Berk, M., and Van Rheenen, T.E. (2021). The mental health and lifestyle impacts of COVID-19 on bipolar disorder. *J. Affect. Disord.* 282, 442–447. <https://doi.org/10.1016/j.jad.2020.12.186>.
9. Merikangas, K.R., Jin, R., He, J.P., Kessler, R.C., Lee, S., Sampson, N.A., Viana, M.C., Andrade, L.H., Hu, C., Karam, E.G., et al. (2011). Prevalence and correlates of bipolar spectrum disorder in the world mental health Survey initiative. *Arch. Gen. Psychiatr.* 68, 241–251. <https://doi.org/10.1001/archgenpsychiatry.2011.12>.
10. Yoshimi, N., Futamura, T., Bergen, S.E., Iwayama, Y., Ishima, T., Sellgren, C., Ekman, C.J., Jakobsson, J., Pålsson, E., Kakumoto, K., et al. (2016). Cerebrospinal fluid metabolomics identifies a key role of

- isocitrate dehydrogenase in bipolar disorder: evidence in support of mitochondrial dysfunction hypothesis. *Mol. Psychiatr.* 21, 1504–1510. <https://doi.org/10.1038/mp.2015.217>.
11. Hutton, P., Taylor, P.J., Mulligan, L., Tully, S., and Moncrieff, J. (2015). Quetiapine immediate release v. placebo for schizophrenia: systematic review, meta-analysis and reappraisal. *Br. J. Psychiatry* 206, 360–370. <https://doi.org/10.1192/bjp.bp.114.154377>.
 12. Katz, I.R., Rogers, M.P., Lew, R., Thwin, S.S., Doros, G., Ahearn, E., Ostacher, M.J., DeLisi, L.E., Smith, E.G., Ringer, R.J., et al. (2022). Lithium treatment in the prevention of repeat suicide-related outcomes in veterans with major depression or bipolar disorder A randomized clinical trial. *JAMA Psychiatr.* 79, 24–32. <https://doi.org/10.1001/jamapsychiatry.2021.3170>.
 13. Vanderplow, A.M., Eagle, A.L., Kermath, B.A., Bjornson, K.J., Robison, A.J., and Cahill, M.E. (2021). Akt-mTOR hypoactivity in bipolar disorder gives rise to cognitive impairments associated with altered neuronal structure and function. *Neuron* 109, 1479–1496.e6. <https://doi.org/10.1016/j.neuron.2021.03.008>.
 14. Gigase, F.A.J., Snijders, G.J., Boks, M.P., and de Witte, L.D. (2019). Neurons and glial cells in bipolar disorder: a systematic review of postmortem brain studies of cell number and size. *Neurosci. Biobehav. Rev.* 103, 150–162. <https://doi.org/10.1016/j.neubiorev.2019.05.027>.
 15. Nabulsi, L., Farrell, J., McPhilemy, G., Kilmartin, L., Dauvermann, M.R., Akudjedu, T.N., Najt, P., Ambati, S., Martyn, F.M., McLoughlin, J., et al. (2022). Normalization of impaired emotion inhibition in bipolar disorder mediated by cholinergic neurotransmission in the cingulate cortex. *Neuropsychopharmacology* 47, 1643–1651. <https://doi.org/10.1038/s41386-022-01268-7>.
 16. Glausier, J.R., Enwright, J.F., and Lewis, D.A. (2020). Diagnosis- and cell type-specific mitochondrial functional pathway signatures in schizophrenia and bipolar disorder. *Am. J. Psychiatr.* 177, 1140–1150.
 17. Zhu, Y., Owens, S.J., Murphy, C.E., Ajulu, K., Rothmond, D., Purves-Tyson, T., Middleton, F., Webster, M.J., and Weickert, C.S. (2022). Inflammation-related transcripts define ? high? and ?low? subgroups of individuals with schizophrenia and bipolar disorder in the midbrain. *Brain Behav. Immun.* 105, 149–159. <https://doi.org/10.1016/j.bbi.2022.06.012>.
 18. Ruderfer, D.M., Ripke, S., McQuillin, A., Boocock, J., Stahl, E.A., Pavlides, J.M.W., Mullins, N., Charney, A.W., Ori, A.P.S., Loohuis, L.M.O., et al. (2018). Genomic Dissection of Bipolar Disorder and Schizophrenia, Including 28 Subphenotypes. *Cell* 173, 1705–1715.e16. <https://doi.org/10.1016/j.cell.2018.05.046>.
 19. Kadriu, B., Farmer, C.A., Yuan, P., Park, L.T., Deng, Z.D., Moaddel, R., Henter, I.D., Shovestul, B., Ballard, E.D., Kraus, C., et al. (2021). The kynurenine pathway and bipolar disorder: intersection of the monoaminergic and glutamatergic systems and immune response. *Mol. Psychiatr.* 26, 4085–4095. <https://doi.org/10.1038/s41380-019-0589-8>.
 20. Chinopoulos, C. (2020). Ant1 mutant mice bridge the mitochondrial and serotonergic dysfunctions in bipolar disorder. *Mol. Psychiatr.* 25, 2203–2204. <https://doi.org/10.1038/s41380-018-0251-x>.
 21. Krams, I.A., Rantala, M.J., Borr az-Le on, J.I., and Luoto, S. (2021). Bipolar disorder: an evolutionary psychoneuroimmunological approach (vol 122, pg 28, 2021). *Neurosci. Biobehav. Rev.* 126, 528.
 22. Miklowitz, D.J., Portnoff, L.C., Armstrong, C.C., Keenan-Miller, D., Breen, E.C., Muscatell, K.A., Eisenberger, N.I., and Irwin, M.R. (2016). Inflammatory cytokines and nuclear factor-kappa B activation in adolescents with bipolar and major depressive disorders. *Psychiatr. Res.* 241, 315–322. <https://doi.org/10.1016/j.psychres.2016.04.120>.
 23. Bay es,  ., Collins, M.O., Reig-Viader, R., Gou, G., Goulding, D., Izquierdo, A., Choudhary, J.S., Emes, R.D., and Grant, S.G.N. (2017). Evolution of complexity in the zebrafish synapse proteome. *Nat. Commun.* 8, 14613. <https://doi.org/10.1038/ncomms14613>.
 24. Mu, X., Liu, J., Wang, H., Yuan, L., Wang, C., Li, Y., and Qiu, J. (2022). Bisphenol F impaired zebrafish cognitive ability through inducing neural cell heterogeneous responses. *Environ. Sci. Technol.* 56, 8528–8540. <https://doi.org/10.1021/acs.est.2c01531>.
 25. Canzian, J., Goncalves, F.L.S., M ller, T.E., Francescon, F., Santos, L.W., Acedara, I.A., and Rosemberg, D.B. (2022). Zebrafish as a potential non-traditional model organism in translational bipolar disorder research: genetic and behavioral insights. *Neurosci. Biobehav. Rev.* 136, 104620. <https://doi.org/10.1016/j.neubiorev.2022.104620>.
 26. Langheinrich, U. (2003). Zebrafish: a new model on the pharmaceutical catwalk. *Bioessays* 25, 904–912. <https://doi.org/10.1002/bies.10326>.
 27. Bahary, N., Goishi, K., Stuckenholtz, C., Weber, G., LeBlanc, J., Schafer, C.A., Berman, S.S., Klagsbrun, M., and Zon, L.I. (2007). Duplicate VegfA genes and orthologues of the KDR receptor tyrosine kinase family mediate vascular development in the zebrafish. *Blood* 110, 3627–3636. <https://doi.org/10.1182/blood-2006-04-016378>.
 28. de Melo Martins, G.M., Petersen, B.D., R bensam, G., da Silva, J.M.K., Gaspar, K.V., Wiprich, M.T., Altenhofen, S., and Bonan, C.D. (2022). Physical exercise prevents behavioral alterations in a reserpine-treated zebrafish: a putative depression model. *Pharmacol. Biochem. Behav.* 220, 173455. <https://doi.org/10.1016/j.pbb.2022.173455>.
 29. Demin, K.A., Meshalkina, D.A., Volgin, A.D., Yakovlev, O.V., de Abreu, M.S., Alekseeva, P.A., Friend, A.J., Lakstygala, A.M., Zabegalov, K., Amstislavskaya, T.G., et al. (2019). Developing zebrafish experimental animal models relevant to schizophrenia. *Neurosci. Biobehav. Rev.* 105, 126–133. <https://doi.org/10.1016/j.neubiorev.2019.07.017>.
 30. Zheng, P., Yang, J., Li, Y., Wu, J., Liang, W., Yin, B., Tan, X., Huang, Y., Chai, T., Zhang, H., et al. (2020). Gut microbial signatures can discriminate unipolar from bipolar depression. *Adv. Sci.* 7, 1902862. <https://doi.org/10.1002/adv.201902862>.
 31. McGuinness, A.J., Davis, J.A., Dawson, S.L., Loughman, A., Collier, F., O’Hely, M., Simpson, C.A., Green, J., Marx, W., C, H., et al. (2022). A systematic review of gut microbiota composition in observational studies of major depressive disorder, bipolar disorder and schizophrenia. *Mol. Psychiatr.* 27, 1920–1935. <https://doi.org/10.1038/s41380-022-01456-3>.
 32. Masadeh, M.M., Alzoubi, K.H., Khabour, O.F., and Al-Azzam, S.I. (2015). Ciprofloxacin-induced antibacterial activity is attenuated by phosphodiesterase inhibitors. *Curr. Ther. Res. Clin. Exp.* 77, 14–17. <https://doi.org/10.1016/j.curtheres.2014.11.001>.
 33. Bhalerao, S., Talsky, A., Hansen, K., Kingstone, E., Schroeder, B., Karim, Z., and Fung, I. (2006). Ciprofloxacin-induced manic episode. *Psychosomatics* 47, 539–540. <https://doi.org/10.1176/appi.psy.47.6.539>.
 34. Abouesh, A., Stone, C., and Hobbs, W.R. (2002). Antimicrobial-induced mania (antibiomania): a review of spontaneous reports. *J. Clin. Psychopharmacol.* 22, 71–81. <https://doi.org/10.1097/00004714-200202000-00012>.
 35. Kato, T.M., Kubota-Sakashita, M., Fujimori-Tonou, N., Saitow, F., Fuke, S., Masuda, A., Itoharu, S., Suzuki, H., and Kato, T. (2018). Ant1 mutant mice bridge the mitochondrial and serotonergic dysfunctions in bipolar disorder. *Mol. Psychiatr.* 23, 2039–2049. <https://doi.org/10.1038/s41380-018-0074-9>.
 36. Zheng, P., Wu, J., Zhang, H., Perry, S.W., Yin, B., Tan, X., Chai, T., Liang, W., Huang, Y., Li, Y., et al. (2021). The gut microbiome modulates gut-brain axis glycerophospholipid metabolism in a region-specific manner in a nonhuman primate model of depression. *Mol. Psychiatr.* 26, 2380–2392. <https://doi.org/10.1038/s41380-020-0744-2>.
 37. Kathuria, A., Lopez-Lengowski, K., Vater, M., McPhie, D., Cohen, B.M., and Karmacharya, R. (2020). Transcriptome analysis and functional characterization of cerebral organoids in bipolar disorder. *Genome Med.* 12, 34. <https://doi.org/10.1186/s13073-020-00733-6>.
 38. Carvalho, A.F., Firth, J., and Vieta, E. (2020). Bipolar disorder. *N. Engl. J. Med.* 383, 58–66. <https://doi.org/10.1056/NEJMra1906193>.
 39. Bauer, M.S. (2022). Bipolar disorder. *Ann. Intern. Med.* 175, ITC97–ITC112. <https://doi.org/10.7326/aitc202207190>.
 40. Ziv, L., Muto, A., Schoonheim, P.J., Meijnsing, S.H., Strasser, D., Ingraham, H.A., Schaaf, M.J.M., Yamamoto, K.R., and Baier, H. (2013). An affective disorder in zebrafish with mutation of the glucocorticoid receptor. *Mol.*

- Psychiatr. 18, 681–691. <https://doi.org/10.1038/mp.2012.64>.
41. Dodd, D., Spitzer, M.H., Van Treuren, W., Merrill, B.D., Hryckowian, A.J., Higginbottom, S.K., Le, A., Cowan, T.M., Nolan, G.P., Fischbach, M.A., and Sonnenburg, J.L. (2017). A gut bacterial pathway metabolizes aromatic amino acids into nine circulating metabolites. *Nature* 551, 648–652. <https://doi.org/10.1038/nature24661>.
 42. Wang, D., Wu, J., Zhu, P., Xie, H., Lu, L., Bai, W., Pan, W., Shi, R., Ye, J., Xia, B., et al. (2022). Tryptophan-rich diet ameliorates chronic unpredictable mild stress induced depression- and anxiety-like behavior in mice: the potential involvement of gut-brain axis. *Food Res. Int.* 157, 111289. <https://doi.org/10.1016/j.foodres.2022.111289>.
 43. Golightly, K.L., Lloyd, J.A., Hobson, J.E., Gallagher, P., Mercer, G., and Young, A.H. (2001). Acute tryptophan depletion in schizophrenia. *Psychol. Med.* 31, 75–84. <https://doi.org/10.1017/s0033291799003062>.
 44. Tian, P., Chen, Y., Zhu, H., Wang, L., Qian, X., Zou, R., Zhao, J., Zhang, H., Qian, L., Wang, Q., et al. (2022). Bifidobacterium breve CCFM1025 attenuates major depression disorder via regulating gut microbiome and tryptophan metabolism: a randomized clinical trial. *Brain Behav. Immun.* 100, 233–241. <https://doi.org/10.1016/j.bbi.2021.11.023>.
 45. Institute of Medicine Committee on Military Nutrition Research (1999). *The Role of Protein and Amino Acids in Sustaining and Enhancing Performance* (National Academies Press).
 46. Lee, W., Kang, B.H., Yang, H., Park, M., Kwak, J.H., Chung, T., Jeong, Y., Kim, B.K., and Jeong, K.H. (2021). Spread spectrum SERS allows label-free detection of atomolar neurotransmitters. *Nat. Commun.* 12, 159. <https://doi.org/10.1038/s41467-020-20413-8>.
 47. Platten, M., Nollen, E.A.A., Röhrig, U.F., Fallarino, F., and Opitz, C.A. (2019). Tryptophan metabolism as a common therapeutic target in cancer, neurodegeneration and beyond. *Nat. Rev. Drug Discov.* 18, 379–401. <https://doi.org/10.1038/s41573-019-0016-5>.
 48. Pu, J., Liu, Y., Zhang, H., Tian, L., Gui, S., Yu, Y., Chen, X., Chen, Y., Yang, L., Ran, Y., et al. (2021). An integrated meta-analysis of peripheral blood metabolites and biological functions in major depressive disorder. *Mol. Psychiatr.* 26, 4265–4276. <https://doi.org/10.1038/s41380-020-0645-4>.
 49. Heilman, P.L., Wang, E.W., Lewis, M.M., Krzyzanowski, S., Capan, C.D., Burmeister, A.R., Du, G., Escobar Galvis, M.L., Brundin, P., Huang, X., and Brundin, L. (2020). Tryptophan metabolites are associated with symptoms and nigral pathology in Parkinson's disease. *Mov. Disord.* 35, 2028–2037. <https://doi.org/10.1002/mds.28202>.
 50. Han, L., Zhao, L., Zhou, Y., Yang, C., Xiong, T., Lu, L., Deng, Y., Luo, W., Chen, Y., Qiu, Q., et al. (2022). Altered metabolome and microbiome features provide clues in understanding irritable bowel syndrome and depression comorbidity. *ISME J.* 16, 983–996. <https://doi.org/10.1038/s41396-021-01123-5>.
 51. Li, X., Zhang, Z.H., Zayed, H.M., Yun, J., Zhang, G., and Qi, X. (2021). An insight into the roles of dietary tryptophan and its metabolites in intestinal inflammation and inflammatory bowel disease. *Mol. Nutr. Food Res.* 65, e2000461. <https://doi.org/10.1002/mnfr.202000461>.
 52. Bartoli, F., Misiak, B., Callovin, T., Cavaleri, D., Cioni, R.M., Crococo, C., Savitz, J.B., and Carrà, G. (2021). The kynurenine pathway in bipolar disorder: a meta-analysis on the peripheral blood levels of tryptophan and related metabolites. *Mol. Psychiatr.* 26, 3419–3429. <https://doi.org/10.1038/s41380-020-00913-1>.
 53. Lai, Y., Liu, C.W., Yang, Y., Hsiao, Y.C., Ru, H., and Lu, K. (2021). High-coverage metabolomics uncovers microbiota-driven biochemical landscape of interorgan transport and gut-brain communication in mice. *Nat. Commun.* 12, 6000. <https://doi.org/10.1038/s41467-021-26209-8>.
 54. Bueno-Carrasco, M.T., Cuéllar, J., Flydal, M.I., Santiago, C., Krákenes, T.A., Kleppe, R., López-Blanco, J.R., Marcilla, M., Teigen, K., Alvira, S., et al. (2022). Structural mechanism for tyrosine hydroxylase inhibition by dopamine and reactivation by Ser40 phosphorylation. *Nat. Commun.* 13, 74. <https://doi.org/10.1038/s41467-021-27657-y>.
 55. Corkrum, M., Covelo, A., Lines, J., Bellocchio, L., Pisansky, M., Loke, K., Quintana, R., Rothwell, P.E., Lujan, R., Marsicano, G., et al. (2020). Dopamine-evoked synaptic regulation in the nucleus accumbens requires astrocyte activity. *Neuron* 105, 1036–1047.e5. <https://doi.org/10.1016/j.neuron.2019.12.026>.
 56. Mayneris-Perxachs, J., Castells-Nobau, A., Arnoriaga-Rodríguez, M., Martín, M., de la Vega-Correa, L., Zapata, C., Burokas, A., Blasco, G., Coll, C., Escrichs, A., et al. (2022). Microbiota alterations in proline metabolism impact depression. *Cell Metabol.* 34, 681–701.e10. <https://doi.org/10.1016/j.cmet.2022.04.001>.
 57. Colasanti, A., Bugiardini, E., Amawi, S., Poole, O.V., Skorupinska, I., Skorupinska, M., Germain, L., Kozyra, D., Holmes, S., James, N., et al. (2020). Primary mitochondrial diseases increase susceptibility to bipolar affective disorder. *J. Neurol. Neurosurg. Psychiatry* 91, 892–894. <https://doi.org/10.1136/jnnp-2020-323632>.
 58. Schneider, M., Levant, B., Reichel, M., Gulbins, E., Kornhuber, J., and Müller, C.P. (2017). Lipids in psychiatric disorders and preventive medicine. *Neurosci. Biobehav. Rev.* 76, 336–362. <https://doi.org/10.1016/j.neubiorev.2016.06.002>.
 59. Ogrodnik, M., Zhu, Y., Langhi, L.G.P., Tchkonina, T., Krüger, P., Fielder, E., Vittorelli, S., Ruswhandi, R.A., Giorgadze, N., Pirtskhalava, T., et al. (2019). Obesity-induced cellular senescence drives anxiety and impairs neurogenesis. *Cell Metabol.* 29, 1061–1077.e8. <https://doi.org/10.1016/j.cmet.2018.12.008>.
 60. Zhanghao, K., Liu, W., Li, M., Wu, Z., Wang, X., Chen, X., Shan, C., Wang, H., Chen, X., Dai, Q., et al. (2020). High-dimensional super-resolution imaging reveals heterogeneity and dynamics of subcellular lipid membranes. *Nat. Commun.* 11, 5890. <https://doi.org/10.1038/s41467-020-19747-0>.
 61. Avila, R.L., Tevlin, B.R., Lees, J.P.B., Inouye, H., and Kirschner, D.A. (2007). Myelin structure and composition in zebrafish. *Neurochem. Res.* 32, 197–209. <https://doi.org/10.1007/s11064-006-9136-5>.
 62. Bazan, N.G. (2005). Lipid signaling in neural plasticity, brain repair, and neuroprotection. *Mol. Neurobiol.* 32, 89–103. <https://doi.org/10.1385/mn:32:1:089>.
 63. Kneussel, M., and Friese, M.A. (2021). SnapShot: neuronal dysfunction in inflammation. *Neuron* 109, 1754–1754.e1. <https://doi.org/10.1016/j.neuron.2021.03.005>.
 64. Bairamian, D., Sha, S., Rolhion, N., Sokol, H., Dorothée, G., Lemere, C.A., and Krantic, S. (2022). Microbiota in neuroinflammation and synaptic dysfunction: a focus on Alzheimer's disease. *Mol. Neurodegener.* 17, 19. <https://doi.org/10.1186/s13024-022-00522-2>.
 65. Nowell, J., Blunt, E., and Edison, P. (2023). Incretin and insulin signaling as novel therapeutic targets for Alzheimer's and Parkinson's disease. *Mol. Psychiatr.* 28, 217–229. <https://doi.org/10.1038/s41380-022-01792-4>.
 66. Novianti, E., Katsuura, G., Kawamura, N., Asakawa, A., and Inui, A. (2021). Attractylenolide-III suppresses lipopolysaccharide-induced inflammation via downregulation of toll-like receptor 4 in mouse microglia. *Heliyon* 7, e08269. <https://doi.org/10.1016/j.heliyon.2021.e08269>.
 67. Falcicchia, C., Tozzi, F., Arancio, O., Watterson, D.M., and Origlia, N. (2020). Involvement of p38 MAPK in synaptic function and dysfunction. *Int. J. Mol. Sci.* 21, 5624. <https://doi.org/10.3390/ijms21165624>.
 68. Patel, R.R., Wolfe, S.A., Bajo, M., Abeynaik, S., Pahng, A., Borgonetti, V., D'Ambrosio, S., Nikzad, R., Edwards, S., Paust, S., et al. (2021). IL-10 normalizes aberrant amygdala GABA transmission and reverses anxiety-like behavior and dependence-induced escalation of alcohol intake. *Prog. Neurobiol.* 199, 101952. <https://doi.org/10.1016/j.pneurobio.2020.101952>.
 69. Hou, L., Fu, Y., Zhao, C., Fan, L., Hu, H., and Yin, S. (2022). Ciprofloxacin and enrofloxacin can cause reproductive toxicity via endocrine signaling pathways. *Ecotoxicol. Environ. Saf.* 244, 114049. <https://doi.org/10.1016/j.ecoenv.2022.114049>.
 70. Qiu, W., Fang, M., Magnuson, J.T., Greer, J.B., Chen, Q., Zheng, Y., Xiong, Y., Luo, S., Zheng, C., and Schlenk, D. (2020). Maternal exposure to environmental antibiotic mixture during gravid period predicts gastrointestinal effects in zebrafish offspring. *J. Hazard Mater.*

- 399, 123009. <https://doi.org/10.1016/j.jhazmat.2020.123009>.
71. Schulz, M., and Schmoldt, A. (2003). Therapeutic and toxic blood concentrations of more than 800 drugs and other xenobiotics. *Pharmazie* 58, 447–474.
 72. Fick, J., Söderström, H., Lindberg, R.H., Phan, C., Tysklind, M., and Larsson, D.G.J. (2009). Contamination of surface, ground, and drinking water from pharmaceutical production. *Environ. Toxicol. Chem.* 28, 2522–2527. <https://doi.org/10.1897/09-073.1>.
 73. Luu, B., and Rodway, G. (2018). Lithium therapy for bipolar disorder. *J. Nurse Pract.* 14, 93–99. <https://doi.org/10.1016/j.nurpra.2017.09.025>.
 74. Benvenuti, R., Marcon, M., Gallas-Lopes, M., de Mello, A.J., Herrmann, A.P., and Piato, A. (2021). Swimming in the maze: an overview of maze apparatuses and protocols to assess zebrafish behavior. *Neurosci. Biobehav. Rev.* 127, 761–778. <https://doi.org/10.1016/j.neubiorev.2021.05.027>.
 75. Schneider, C.A., Rasband, W.S., and Eliceiri, K.W. (2012). NIH Image to ImageJ: 25 years of image analysis. *Nat. Methods* 9, 671–675. <https://doi.org/10.1038/nmeth.2089>.
 76. Ranjbarvaziri, S., Kooiker, K.B., Ellenberger, M., Fajardo, G., Zhao, M., Vander Roest, A.S., Woldeyes, R.A., Koyano, T.T., Fong, R., Ma, N., et al. (2021). Altered cardiac energetics and mitochondrial dysfunction in hypertrophic cardiomyopathy. *Circulation* 144, 1714–1731. <https://doi.org/10.1161/CIRCULATIONAHA.121.053575>.
 77. Wang, X., Qiu, J., Xu, Y., Liao, G., Jia, Q., Pan, Y., Wang, T., and Qian, Y. (2021). Integrated non-targeted lipidomics and metabolomics analyses for fluctuations of neonicotinoids imidacloprid and acetamiprid on Neuro-2a cells. *Environ. Pollut.* 284, 117327. <https://doi.org/10.1016/j.envpol.2021.117327>.
 78. Zhao, T., Zhang, C., Zhong, S., Chen, Q., Liu, S., Jiao, W., Liu, W., Huang, L., Zhang, Y., and Zhang, Y. (2022). Synergistic alleviation effects of anchovy hydrolysates-catechin on scopolamine-induced mice memory deficits: the exploration of the potential relationship among gut-brain-axis. *Food Funct.* 13, 1563–1578. <https://doi.org/10.1039/d1fo02195h>.
 79. Pan, J.X., Xia, J.J., Deng, F.L., Liang, W.W., Wu, J., Yin, B.M., Dong, M.X., Chen, J.J., Ye, F., Wang, H.Y., et al. (2018). Diagnosis of major depressive disorder based on changes in multiple plasma neurotransmitters: a targeted metabolomics study. *Transl. Psychiatry* 8, 130. <https://doi.org/10.1038/s41398-018-0183-x>.
 80. Liu, P., Weng, R., Sheng, X., Wang, X., Zhang, W., Qian, Y., and Qiu, J. (2020). Profiling of organosulfur compounds and amino acids in garlic from different regions of China. *Food Chem.* 305, 125499. <https://doi.org/10.1016/j.foodchem.2019.125499>.
 81. Chen, C., Chen, H., Zhang, Y., Thomas, H.R., Frank, M.H., He, Y., and Xia, R. (2020). TBtools: an integrative toolkit developed for interactive analyses of big biological data. *Mol. Plant* 13, 1194–1202. <https://doi.org/10.1016/j.molp.2020.06.009>.

STAR★METHODS

KEY RESOURCES TABLE

REAGENT or RESOURCE	SOURCE	IDENTIFIER
Antibodies		
Rabbit anti-GFAP	Proteintech	Cat. # 16825-1-AP; RRID: AB_2109646
Rabbit anti-NeuN	Proteintech	Cat. # 26975-1-AP; RRID: AB_2880708
Rabbit anti-Iba-1	Proteintech	Cat. # 10904-1-AP; RRID: AB_2224377
Rabbit anti-Synaptophysin	Abcam	Cat. # ab32594; RRID: AB_778204
Mouse anti-Beta-Actin (Clone, mouse 2D4H5)	Proteintech	Cat. #66009-1-IG; RRID: AB_2687938
Rabbit anti-JNK1 + JNK2 + JNK3(Clone, rabbit EPR16797-211)	Abcam	Cat. #ab179461; RRID: AB_2744672
Rabbit anti-Phospho-SAPK/JNK (Thr183/Tyr185)	Cell Signalling Technology	Cat. #4668T
Rabbit anti-p38 MAPK	Proteintech	Cat. #14064-1-AP; RRID: AB_2878007
Chemicals, peptides, and recombinant proteins		
Methanol	Fisher	Cat. #A456-4; CAS:67-56-1
Acetonitrile	Fisher	Cat. #A955-4; CAS:75-05-8
Formic acid	Fisher	Cat. #A117-50; CAS:64-18-6
Ciprofloxacin	Dr. Ehrenstorfer	Cat. #DRE-C11668500; CAS:93107-08-5
Lithium carbonate	Macklin	Cat. #L812282; CAS:554-13-2
L-phenylalanine	First Standard	Cat. #1ST1414; CAS: 63-91-2
Gamma-aminobutyrate	First Standard	Cat. #1ST7512; CAS: 56-12-2
Epinephrine	First Standard	Cat. #1ST000565; CAS: 51-43-4
Indole	First Standard	Cat. # 1ST24020; CAS: 120-72-9
Indole-3-acetate	First Standard	Cat. #1ST24030; CAS: 133-32-4
Glutamine	First Standard	Cat. #1ST1407; CAS: 56-85-9
Norepinephrine	First Standard	Cat. #1ST000564; CAS: 51-41-2
Arginine	First Standard	Cat. #1ST1402; CAS: 74-79-3
5-hydroxy-L-tryptophan	First Standard	Cat. #1ST14864; CAS: 4350-09-8
Acetylcholine	First Standard	Cat. #1ST163136; CAS: 60-31-1
L-glutamate	First Standard	Cat. #1ST1406; CAS: 56-86-0
L-tryptophan	First Standard	Cat. #1ST1418; CAS: 73-22-3
Proline	First Standard	Cat. #1ST1415; CAS: 147-85-3
Tyramine	First Standard	Cat. #1ST40050; CAS: 51-67-2
Dopamine	First Standard	Cat. #1ST1322A; CAS: 62-31-7
5-hydroxyindoleacetate	First Standard	Cat. #1ST000316; CAS:54-16-0
Kynurenine	First Standard	Cat. #1ST8338; CAS:2922-83-0
L-tyrosine	First Standard	Cat. #1ST1419; CAS: 60-18-4
Serotonin	First Standard	Cat. #1ST157682; CAS: 50-67-9
Choline	First Standard	Cat. #1ST1536; CAS: 67-48-1
Tryptamine	First Standard	Cat. #1ST001616; CAS: 61-54-1
Critical commercial assays		
Protein extraction kit	Solarbio	Cat. #R0050
BCA protein assay kit	Beyotime	Cat. #P0011
Fish IL-6 ELISA kits	Jiancheng	Cat. #H007-1-1

(Continued on next page)

Continued

REAGENT or RESOURCE	SOURCE	IDENTIFIER
Fish IL-1 β ELISA kits	Jiancheng	Cat. #H002-1-1
Fish TNF α ELISA kits	Jiancheng	Cat. #H052-1-1
TRIzol reagent	Foregene	Cat. #RE-03014
All-in-One First-Strand Synthesis MasterMix (with dsDNase) Kit	Kemix	Cat. #KR0501
2 \times SYBR Green qPCR Premix kit	Kemix	Cat. # KS0601
Wes Separation Capillary Cartridges	ProteinSimple	Cat. #PDM-001 +SM-W004

Deposited data

mRNA-seq data	This paper	NCBI Sequence Read Archive, accession ID PRJNA940583
Metabolomics data	This paper	See Table S3
Lipidomics data	This paper	See Table S4

Experimental models: Organisms/strains

Zebrafish: wild-type AB strain	Eze-Rinka Company, Nanjing, China	N/A
--------------------------------	-----------------------------------	-----

Oligonucleotides

Refer to Table S2	This paper	N/A
-----------------------------------	------------	-----

Software and algorithms

ImageJ	Schneider et al.2012 ⁷⁵	https://imagej.nih.gov/ij/
Compound Discover version 3.3	Thermo Fisher	https://www.thermofisher.cn/cn/zh/home/industrial/mass-spectrometry/liquid-chromatography-mass-spectrometry-lc-ms/lc-ms-software/multi-omics-data-analysis/compound-discoverer-software.html
Progenesis QI version 4.0	Waters	https://www.nonlinear.com/progenesis/qi/
TBtools	Chengjie Chen et al.2020 ⁸¹	https://github.com/CJ-Chen/TBtools
MassLynx	Waters	https://www.waters.com/waters/en_US/MassLynx-MS-Software/nav.htm?cid=513662
SPSS version 25.0	IBM	https://www.ibm.com/cn-zh/spss
GraphPad Prism 8.0	GraphPad	https://www.graphpad.com/scientific-software/prism/

Other

Waters application note	Waters	https://www.waters.com/content/dam/waters/en/app-notes/2011/720004107/720004107-zh.pdf
mz cloud	Thermo Fisher	https://www.mzcloud.org
Human Metabolome Database	HMDB	http://www.hmdb.ca
Lipidmaps	Lipidmaps	http://www.lipidmaps.org
bioinformatic platform	bioinformatics	https://www.bioinformatics.com.cn
IMPala version 13	Cloudera	http://impala.molgen.mpg.de
MetaboAnalyst	MetaboAnalyst	https://www.metaboanalyst.ca/

RESOURCE AVAILABILITY**Lead contact**

Further information and requests for resources and reagents should be directed to and will be fulfilled by the Lead Contact, Prof. Jing Qiu (qiuqing@caas.cn).

Materials availability

This study did not generate new unique reagents.

Data and code availability

- The metabolomics and lipidomics data have been uploaded as separate excel files in [Tables S3](#) and [S4](#) respectively, the mRNA-seq data generated in this study have been deposited into the NCBI Sequence Read Archive (SRA), and accession number (SRA:PRJNA940583) was listed in the [key resources table](#). All data reported in this paper will be shared by the [lead contact](#) upon request.
- This paper does not report original code.
- Any additional information required to reanalyze the data reported in this paper is available from the [lead contact](#) upon request.

EXPERIMENTAL MODEL AND SUBJECT DETAILS

Given that BD is more prevalent in females than in males,^{5,6} female zebrafish were selected for this study. Adult female zebrafish (wild-type AB strain) at early sexual maturity (90 days post fertilization [dpf]) used in this experimentation were purchased from Eze-Rinka Company (Nanjing, China). After 2 weeks of clear water domestication, female zebrafish were exposed to 100 and 1000 µg/L of ciprofloxacin for 4 weeks. Exposure concentrations were selected on the previous studies and the levels to which humans are exposed through diet or treatment.^{69–72} In addition, to validate the reliability of the CIP-induced BD-like zebrafish model, a 2-week treatment experiment with lithium carbonate, a mood stabiliser commonly used to treat bipolar disorder, was carried out on zebrafish exposed to 4 weeks of CIP. The exposure concentration for lithium carbonate was 0.02 µg/L, chosen based on the therapeutic dose received by humans during initial treatment.⁷³ Three replicate aquaria (26 cm*14 cm*18 cm) were included per condition, each consisting of 3 L of exposure solution (mother liquor at 20,000 mg/L and pure water as cosolvent), and 25 zebrafish with a control group were run in parallel. Half the volume of the exposure solution was renewed daily to maintain the appropriate concentration of ciprofloxacin. Following a 4-week exposure, the zebrafish were euthanised by immersing in ice water for 30 min. The surface of the euthanised zebrafish were then quickly dried using sterile absorbent paper and placed on a sterile petri dish under a dissecting microscope (Stemi-2000, Zeiss). Using micro-dissecting scissors and fine forceps under the dissecting microscope, the mandible and skull were sequentially removed along the midline of the mouth until whole brain was isolated, collected in cryovials, treated with liquid nitrogen for 5 minutes and stored at a –80 °C freezer prior to analysis.

Our experimental design and procedures were in accordance with the 3R principles. The animals were raised under the following conditions: 28.5 °C and a daily 14:10 h light–dark cycle. For dietary administration, we consistently fed all zebrafish the same sterile hatched brine shrimp (*Artemia* sp.) three times a day, providing approximately 1 mL of brine shrimp per 25 fish at a time, and allowed them to feed *ad libitum*. During the exposure period, it was ensured that the zebrafish in the exposed and control groups fed normally and no mortality occurred. This work has received approval for research ethics from the Independent Animal Ethics Committee of the Chinese Academy of Agricultural Sciences.

METHOD DETAILS

Behavioral assay

We used novel tank test (NTT)⁷⁴ for the behavioural analysis of zebrafish. The experimental setup used in this study was a circular plexiglass container (12.5 cm in diameter) and a rectangular glass tank (13 cm*10 cm*13 cm). In this case, the circular glass container was divided equally into a central zone and a marginal zone by concentric divisions, and the internal space of the rectangular glass tank was divided into a top zone and a bottom zone. The behaviour of zebrafish (CIP-H, n = 6; CIP-L, n = 6; control, n = 6) that had been acclimatised in the container for at least 30 min was automatically tracked using EthoVision XT14 (Wageningen, Netherlands) and a Logitech-C920 camera, which recorded the movement of zebrafish for 5 min. The videos were further analysed using Noldus (Wageningen, Netherlands) to quantify the spatial exploration behaviour of zebrafish used to assess behavioural phenotypes associated with BD. In particular, the behavioural indicators for manic-like behaviour (movement trajectory, frequency of occurrence of manic-like behaviour) and indicators for depressive-like behaviour (total duration and frequency of movement towards the central and top area).

Histological assessments

Fresh whole brain samples (BD, $n = 3$; control, $n = 3$) were washed with normal saline followed by overnight fixation in 4% paraformaldehyde. Then, tissues were embedded in paraffin and sectioned to a thickness of 7 μm . After deparaffinization, sections were stained with haematoxylin and eosin (H&E) to assess overall histomorphology and with Nissl staining to evaluate neuronal morphology. Histopathological images were taken using a light microscope and analysed quantitatively by ImageJ⁷⁵ (version 1.51). All experiments were performed by Baiqiandu Technology Co., Ltd. (Wuhan, China).

RNA-seq analysis from brain samples

In exploring the pathogenesis of BD, whole brains from the female zebrafish were collected in three biological replicates ($n = 3$) per treatment, with each replicate pooling the brains of at least three individuals. Total RNA was isolated and purified using TRIzol reagent (Invitrogen, Carlsbad, CA, USA), following the manufacturer's procedure. The amount and purity of each RNA sample were quantified using a NanoDrop ND-1000 (NanoDrop, Wilmington, DE, USA). RNA purified from brain tissues as indicated was converted into cDNA libraries using the TrueLib mRNA library prep kit for Illumina (ExCell, Bio, China). Library quality was assessed using an Agilent 2100 Bioanalyzer. Sequencing was performed on a MGISEQ-200 sequencer at Shenggong Bioengineering Co., Ltd. (Shanghai, China).

Untargeted metabolomic analysis

A modified sample processing method^{53,76} was used to extract metabolites from the whole brain. The samples were allowed to thaw on ice (one sample contained brain tissue from five individuals, approximately 30 mg, BD, $n = 6$; control, $n = 6$), and 1.5 mL of pre-chilled methanol/water (1:1, v/v) mixture was added. The mixtures were sonicated on an ice bath for 10 min and centrifuged at 15,300 rpm for 10 min at 4 °C. Then, the supernatant and bottom solids were collected after centrifugation. Finally, the supernatant was used to obtain the metabolites for analysis, and the bottom solids were used to obtain lipids for analysis.

The supernatant was evaporated at 45 °C under a constant stream of nitrogen until dryness and re-dissolved in 120 μL of methanol/water (1:1, v/v) complex solution, vortexed vigorously until completely dissolved and centrifuged at 10,000 rpm for 10 min at room temperature. The supernatant was aspirated and placed on a Q-Exactive Orbitrap mass spectrometer for untargeted metabolomic data acquisition. The QC samples were prepared by mixing equal quantities of supernatants from all the analytical samples.

Chromatographic separation was achieved using an Ultimate 3000 UHPLC system (Dionex, USA) coupled with an Xbridge C18 column (2.1 mm \times 100 mm \times 3.5 μm , Waters) at 40 °C. Mass spectrometric detection was performed using a Q-Exactive Orbitrap mass spectrometer equipped with an ESI ion source operated in positive and negative ion mode (Thermo Scientific, Waltham, MA). The Chromatographic and ion source parameters have been described in detail in the study by Wang X et al⁷⁷ in our laboratory. In brief, chromatographic separation of the metabolites was obtained with gradient elution of Acetonitrile/water (40:60, v/v) with 10 mM ammonium acetate and isopropanol/acetonitrile (9:1, v/v) with 10 mM ammonium acetate. Furthermore, the ion scan range was adjusted to 50–1200 m/z. The total ion chromatogram of untargeted metabolomic in positive and negative ion mode were shown in Figures S1A and S1B.

Untargeted lipidomic analysis

1.6 mL of pre-cooled dichloromethane/methanol (3:1, V/V) mixture was added to the obtained bottom solids obtained. The mixtures were sonicated on an ice bath for 20 min and centrifuged at 15,300 rpm for 10 min at 4 °C. Then, the supernatant was collected after centrifugation. The supernatant was evaporated at 45 °C under a constant stream of nitrogen until dryness and re-dissolved in 120 μL of methanol/water (1:1, V/V) complex solution, vortexed vigorously until completely dissolved and centrifuged at 10,000 rpm for 10 min at room temperature. The supernatant was aspirated and placed on Waters SYNAPT XS high-resolution mass spectrometer (Waters, Milford, MA, USA) for untargeted lipidomic data acquisition. The QC samples were prepared by mixing equal quantities of the supernatants from all analytical samples.

The analytical method and instrument parameters for collecting lipid data were performed in accordance with Waters application note (<https://www.waters.com/content/dam/waters/en/app-notes/2011/720004107/720004107-zh.pdf>) with several modifications. Chromatographic separation was achieved using a Waters Acquity

UPLC H-class system (Waters, USA) coupled with an ACQUITY UPLC CSH C18 column (2.1 mm × 100 mm × 1.7 μm, Waters) at 55 °C. Mass spectrometric detection was performed on a SYNAPT XS high-resolution mass spectrometer equipped with an ESI ion source operated in positive and negative ion mode (Waters, USA). The total ion chromatogram of untargeted lipidomic in positive and negative ion mode were shown in [Figures S2A](#) and [S2B](#).

Targeted metabolomic analysis

A modified sample processing method^{78,79} was used to extract metabolites from the whole brain. Samples were allowed to thaw on ice (one sample contained approximately 40–50 mg of brain tissue from seven zebrafish, BD, n = 6; control, n = 6), and 200 μL of pre-cooled 10% formic acid in methanol and 200 μL of pure water were added sequentially. The mixtures were sonicated on an ice bath for 10 min and centrifuged at 15,300 rpm for 10 min at 4 °C. The supernatant was collected after centrifugation. The supernatant was evaporated to dryness at 45 °C under a constant stream of nitrogen, redissolved in 400 μL of a methanol/water (1:1, V/V) solution containing 0.1% formic acid, vortexed vigorously until completely dissolved and centrifuged at 10,000 rpm for 10 min at room temperature. The supernatant was aspirated and placed on an AB Sciex QTRAP 6500 mass spectrometer (Sciex, Ontario, Canada) for targeted metabolomic data acquisition.

The analytical methods and instrument parameters have been described in detail in the study by Liu, P. et al⁸⁰ in our laboratory. Chromatographic separation was achieved using a SCIEX QTrap 6500+ MS/MS system (SCIEX, USA) coupled with an Xbridge C18 column (4.6 mm × 150 mm, 3.5 μm; Waters) at 40 °C. Mass spectrometric detection was performed on the multiple reaction monitoring (MRM) mode equipped with an ESI ion source operated in positive and negative ion mode (SCIEX, USA). Aqueous phase and organic phase were 0.1% formic acid in distilled water and 0.1% formic acid in acetonitrile with gradient elution, respectively. In addition, monitoring ion pair information is listed in [Table S1](#). The total ion chromatogram of targeted metabolomic in positive and negative ion mode were shown in [Figure S3](#).

Transmission electron microscopy (TEM)

Fresh whole brain samples (BD, n = 3; control, n = 3) were collected and rapidly fixed in glutaraldehyde for 24 h. Then, the tissues were embedded, sectioned and stained in accordance with the operating instructions of Baiqiandu Technology Co., Ltd. (Wuhan, China). Images of synaptic ultrastructure of midbrain were taken using TEM. For each well-defined synapse, the length and thickness of the postsynaptic density (PSD) were quantified using ImageJ (version 1.51).

Quantitative real-time PCR (qPCR) analysis

Total RNA was extracted from whole brain samples (one sample contained approximately 15 mg of brain tissue from three zebrafish, BD, n = 3; control, n = 3) by TRIzol reagent (Foregene, Cat. #RE-03014) and then reverse transcribed into cDNA using the All-in-One First-Strand Synthesis MasterMix (with dsDNase) Kit (Kemix, Cat. #KR0501) following the manufacturer's instructions. Next, mRNA levels were detected by standard real-time polymerase chain reaction (RT-PCR). RT-PCR was performed using a 7500 real-time PCR system (Applied Biosystems, USA) with 2×SYBR Green qPCR Premix kit (Kemix, Cat. # KS0601) to measure mRNA expression, with β-actin as a reference gene. Relative quantification of gene amplification by RT-PCR was performed using cycle threshold values. The relative mRNA expression of the selected genes was normalised to the control gene β-actin and determined using the 2^{-ΔΔCt} method. All primer sequences are listed in [Table S2](#).

Immunostaining of brain sections

Fresh whole brain samples (BD, n = 3; control, n = 3) were washed with normal saline and then fixed with 10% formalin for 24 h. Brain sections were prepared using a frozen sectioning machine (Leica, RM 2016). Anti-rabbit GFAP (Proteintech, Cat. # 16825-1-AP), anti-rabbit NeuN (Proteintech, Cat. # 26975-1-AP), anti-rabbit Iba-1 (Proteintech, Cat. # 10904-1-AP), anti-rabbit Synaptophysin (Abcam, Cat. # ab32594) and fluorescent secondary antibody were used for immunostaining of brain sections obtained from control and BD groups. The cell nuclei were visualised using DAPI. Representative images of the midbrain region were obtained using a fluorescence microscope (Leica, DM 3000) and an inverted confocal microscope (Olympus, FV1200). Preparation, staining and imaging of midbrain were completed by Jingzhun Test Technology Co., Ltd. (Beijing, China).

Western blotting

Protein extraction and quantitative analysis were performed according to the supplier's instructions. For frozen zebrafish whole brain samples (one sample contained approximately 30 mg of brain tissue from five zebrafish, BD, $n = 3$; control, $n = 3$), cytoplasmic and nuclear proteins were extracted from the samples using a protein extraction kit (Solarbio, Cat. #R0050). BCA protein assay kit (Beyotime, Cat. #P0011) was used to determine protein concentrations. Western blotting was performed using the Wes-Simple Western system, an automated capillary-based size-sorting system containing an anti-rabbit detection module for Wes and a Wes Separation Capillary Cartridges for 12 to 230 kDa (ProteinSimple, Cat. #PDM-001 + SM-W004). Protein expression was measured by chemiluminescence and quantified as the area under the peak of the chemiluminescence chromatogram using Compass (ProteinSimple, USA). Proteins were detected using the following primary antibodies: GFAP (Proteintech, Cat. #16825-1-AP), NeuN (Proteintech, Cat. #26975-1-AP), Iba-1 (Proteintech, Cat. #10904-1-AP), Synaptophysin (Abcam, Cat. #ab32594), β -Actin (Proteintech, Cat. #66009-1-IG), Anti-JNK1 + JNK2 + JNK3 (Abcam, Cat. #ab179461), Phospho-SAPK/JNK (Cell Signalling Technology, Cat. #4668T), p38 MAPK (Proteintech, Cat. #14064-1-AP) and Phospho-p38 MAPK (Cell Signalling Technology, Cat. #4511T).

Enzyme-linked immunosorbent assay (ELISA)

The levels of three inflammatory cytokines (IL-6, IL-1 β and TNF α) in whole brain samples (one sample contained approximately 30 mg of brain tissue from five zebrafish, BD, $n=3$; control, $n=3$) were analysed using an ELISA according to the manufacturer's instructions. Brain tissues were homogenized in phosphate-buffered saline at a ratio of 1:15 (mg/ μ L) on ice. The supernatant was collected after centrifugation at 2500 rpm/min for 25 min at 4 °C. ELISA kits (IL-6, TNF α and IL-1 β) were obtained from Jiancheng Biochemical Inc., Ltd. (Nanjing, China).

QUANTIFICATION AND STATISTICAL ANALYSIS

mRNA-seq analysis

Gene expression levels were estimated by calculating the value of transcripts per kilobase million. Genes with an FDR-corrected P -value < 0.05 were selected for further investigation. Then, we analysed the enrichment of differentially expressed genes using GO enrichment analysis and the Kyoto Encyclopaedia of Genes and Genomes (KEGG) pathway analysis.

Untargeted metabolomic and lipidomic analysis

Untargeted metabolomic and lipidomic data were collected for compound identification and statistical analysis. Raw untargeted metabolomic and lipidomic data were imported into Compound Discover (version 3.3, Thermo, USA) and Progenesis Q1 (version 4.0, Waters, USA), respectively. The pre-processed procedure of lipidomic and metabolomic data analysis included peak filtering, peak alignment, peak identification and peak intensity integration. For metabolomic analysis in Compound Discoverer 3.3, metabolites were identified against the mz cloud (<https://www.mzcloud.org>) and Human Metabolome Database (<http://www.hmdb.ca>) with a retention time tolerance of 0.2 min, a mass tolerance of 5 ppm, a signal-to-noise ratio of 3, a minimum peak intensity of 1,000,000 and an intensity tolerance of 30%. By contrast, for lipidomic analysis in Progenesis Q1 version 4.0, lipids were identified against the Progenesis Q1 self-contained lipid library and Lipidmaps (<http://www.lipidmaps.org>) database with a minimum abundance of 1000, and the maximum coefficient of variation (standard deviation/mean) was 0.8. Lipids of interest were formally identified by matching fragment spectra, retention times and collision cross-section from the database.

For statistical analysis of untargeted lipidomic, untargeted metabolomic and transcriptomic Cluster heat maps were constructed by TBtools⁸¹ (<https://github.com/CJ-Chen/TBtools>). Volcano maps were analysed and presented by GraphPad Prism 8.0 (San Diego, CA, USA). The results of principal component analysis (PCA) and pathway enrichment analysis were analysed by MetaboAnalyst (<https://www.metaboanalyst.ca/>). Chord plot was plotted using a bioinformatic platform (<https://www.bioinformatics.com.cn> [last accessed on 30 July 2022]), an online platform for data analysis and visualisation.

Targeted metabolomic analysis

Data acquisition and analysis were controlled using MassLynx (version 4.1, Waters, USA), and the results are reported as the integrated area of the chromatographic peak for each metabolite. Chromatographic peak integration was manually verified to ensure consistent peak integration across all samples.

Integrated analysis using metabolites, lipids and transcripts

The biological pathways of key molecules that manifested significant differences between BD zebrafish and controls were annotated. Biological pathway analysis was performed by using MetaboAnalyst (<https://www.metaboanalyst.ca/>) and IMPaLA version 13 (build June 2021) (Integrated Molecular Pathway-Level Analysis) (<http://impala.molgen.mpg.de>) online tools for joint pathway analysis of metabolites, lipids and genes of interest, considering only pathways with false discovery rate (FDR) less than 0.05.

Statistical analysis

Statistical analysis was performed using SPSS (SPSS version 25.0, SPSS Inc, IL) or GraphPad Prism 8.0 (version 8.0, <https://www.graphpad.com/scientific-software/prism>) to calculate *P*-values. Statistical analyses comparing two parameters (between controls and BD) were performed using the unpaired two-tailed Student's *t*-test or the Wilcoxon Rank Sum Test. *P* < 0.05 was considered as significant. Data were calculated using Excel, and data were presented as the mean \pm standard error of the mean (SEM). Graphs were generated using GraphPad Prism 8.0.